INSTITUTO SUPERIOR TÉCNICO
Universidade Técnica de Lisboa

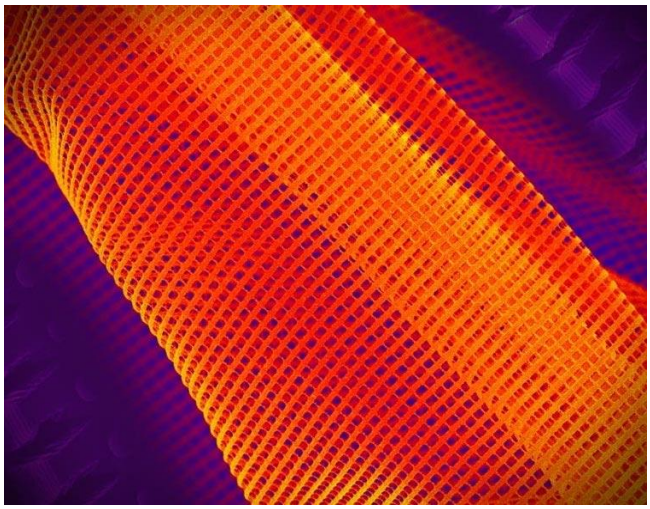

Metamaterials and Double Negative (DNG) Media:
General Properties of Unbounded Media and Guided Wave Propagation

Tiago Augusto Matos Moura

Dissertation submitted to obtain the Master Degree in

Electrical and Computer Engineering

Jury

President:	Professor José Manuel Bioucas Dias
Supervisor:	Professor António Luís Campos da Silva Topa
Co- Supervisor:	Professor Carlos Manuel dos Reis Paiva
Member	Professor Maria João Martins

December 2011

Abstract

Complex media and metamaterials suggest promising applications in electromagnetics. These media can generate new effects in several propagation canonical problems and has attracted great interest from the electromagnetics research community.

In this present work, electromagnetic waves are studied in a media with negative permeability and negative permittivity, called DNG media or DNG metamaterials. This media has some new proprieties like negative refraction and the appearance of backward waves.

First an unbounded DPS-DNG interface is studied. Due to the fact that a negative medium cannot have negative energy density, that would appear in a lossless case, dispersion is considered with the Lorentz Dispersion Model. Domains of existence of TE and TM modes in metamaterials are also analyzed for a less theoretical view of DNG media.

Finally, we analyze a DNG slab interface, with unlimited DPS media as outer medium,where are shown the existence of super slow modes and mode bifurcation.

Keywords

Backward Waves, Double Negative Media, Metamaterials, Microwaves, Negative Refraction, Planar Waveguides, Photonics

Sumário

Meios complexos e metamateriais sugerem aplicações promissoras em electromagnetismo. Estes meios podem gerar novos efeitos em vários conceitos sólidos de propagação.

Recentemente, o índice de refracção negativo, tem atraído enorme interesse da comunidade científica na área do electromagnetismo.

Nesta dissertação, as ondas electromagnéticas são estudadas em meios com permeabilidade e permitividade negativas, chamados de meios duplamente negativos ou meios DNG. Estes meios têm mostrado novas propriedades como a refracção negativa e o surgimento de ondas regressivas.

Primeiramente, estudou-se uma interface simples e ilimitada entre um meio DPS e um meio DNG. Dado que se não fosse considerada a dispersão, teríamos problemas fundamentais que não temos nos meios duplamente positivos, como a densidade de energia negativa, a dispersão é considerada recorrendo ao Modelo Dispersivo de Lorentz. Bandas de existência de propagação de modos TE e TM em metamaterais são também analisados para uma visão menos teórica dos meios DNG.

Em último, é analisada uma placa constituída por um meio DNG entre dois meios DPS ilimitados, onde, nesta interface, é mostrada a existência de modos super lentos e bifurcação de modos.

Palavras Chave

Ondas Regressivas, Meios Duplamente Negativos, Metamateriais, Microondas, Refracção Negativa, Guias de Onda Planares, Fotónica

Acknowledgments

It is difficult to overstate my gratitude to Professor António Topa. His great support, time and patience given during the development of the present work were crucial. His dedication in class, sharpened my taste for Telecommunications. Also, I can not thank enough Professor Carlos Paiva for his inspiration and great efforts to explain things clearly and simply. His classes of Fotónica, piqued my interest in the subject that was hitherto unknown to me.

To my parents, to whom I dedicate this work, for they unconditional support and belief. Without them, this project would be sentenced to failure from the beginning. I can not forget my grandparents, who unfortunately did not saw the end of this work personally, but always believed in its conclusion. I would also like to thank my cousin and uncle for their support and uplifting words, my godmother for support and advice and to my grandfather for developing in me an interest for electronics and telecommunications from early age.

To all my colleagues who have accompanied me during my (long) passage through IST. They are, in an irrelevant order: Priyá Dessai, Tiago Saraiva, Miguel Matos, João Pereira and Cláudia Gomes, between many others. Not forgetting Alexandre and Márolo whose lunch company would always generate a nice discussion on various topics. I am grateful to Filipa Prudêncio and José Alves for their knowledge during the elaboration of this work.

I wish to thank in addition to my friends who, along the years, cheered me with their companionship and followed my journey outside IST: Guilherme Almeida, Marta Miranda, Tiago Galvão and all the others who have passed through.

In substance, to all.

Contents

List of Figures

List of Tables

List Of Symbols

c	Velocity of light
f	Frequency
ω	Angular Frequency
ε	Permittivity
μ	Permeability
v_p	Phase Velocity
v_g	Group Velocity
χ_e	Electric Susceptibility
χ_m	Magnetic Susceptibility
k_0	Vacuum Wave Number

k	Wave Number
n	Refractive Index
η	Wave Impedance
E_0	Initial Electric Field Intensity
H_0	Initial Magnetic Field Intensity
$\mathbf{E}$	Electric Field Intensity
$\mathbf{H}$	Magnetic Field Intensity
$\mathbf{D}$	Electric Flux Density
$\mathbf{B}$	Magnetic Flux Density
η_0	Vacuum Wave Impedance
ζ	Normalized Wave Impedance
$\mathbf{S}_\omega$	Poynting Vector Mean Value
$\mathbf{S}$	Poynting Vector

κ	Extinction Coefficient
$\langle W_e \rangle$	Time Average Electric Energy Density
$\langle W_m \rangle$	Time Average Magnetic Energy Density
$\omega_{0e,m}$	Resonance Frequency
$\omega_{pe,m}$	Plasma Frequency
$\Gamma_{e,m}$	Collision Frequency
$\langle W \rangle$	Average Energy Density
β	Propagation Constant
α	Attenuation Constant
F	Filling Factor
ω_0	Magnetic Resonance Frequency
h	Transverse Wave Number
a	Square of the Relation Between ω_0 and ω_p

$\bar{n}$	Modal Refraction Index
V	Normalized Frequency
d	Thickness of Dielectric Slab
ε_0	Vacuum Permittivity Constant
μ_0	Vacuum Permeability Constant

Nomenclature

DNG	Double Negative
DPS	Double Positive
SNG	Simple Negative
ENG	Epsilon Negative
MNG	Mu Negative
LDM	Lorentz Dispersive Model
TE	Transverse Electric
TM	Transverse Magnetic
NRI	Negative Refraction Index

Chapter 1

Introduction

In this chapter, an overview about the historical background on the subject of this dissertation is made. Being the main researchers and their publications referred. The state of the art of complex media is shown in order to see what research and industry has to offer in present day. Motivations and objectives of this dissertation are explained, followed by it's organization and structure as well as the original contributions.

1.1 Historical Background and Framework

1.1.1 A Brief History of Electricity and Electromagnetism

Since the dawn of Mankind, before any knowledge about electricity, humans were aware of it's existence through shocks from electric fish. Texts dating dating from 2750 BC, written by Egyptians, referred to these fish as "Thunderer of the Nile". Naturalists and physicians from other ancient civilizations that followed, Greek, Roman and Arabic, reported about this fish [1]. Most notably, the Romans Pliny the Elder (23 AD) and Scribonius Largus (47 AD), knew that

such shocks could travel along conducting objects [2]. The earliest and nearest approach to the discovery of the identity of lightning and electricity from any other source, is attributed to the Arabs, who, before the 9th century, had the Arabic word for lightning, *raad*, applied to the electric ray [3].

Ancient cultures around the Mediterranean knew that certain objects, such as rods of amber, could be rubbed with cat's fur to attract light objects like feathers. Thales of Miletos (624 BC) made a series of observations on static electricity around 600 BC, concluding that friction rendered amber magnetic, in contrast to minerals such as magnetite, which needed no rubbing [4]. Such conclusion, in believing the attraction was due to a magnetic effect, was incorrect, but later science would prove a link between magnetism and electricity. From a controversial theory, the Parthians may have had some knowledge about electroplating, based on the 1936 discovery of the Baghdad Battery, which resembles a galvanic cell, though it is uncertain whether the artifact was electrical in nature [5].

Electricity would remain little more than an intellectual curiosity for millennia until 1600, when the English scientist William Gilbert made a careful study of electricity and magnetism, distinguishing the lodestone effect from static electricity produced by rubbing amber [4]. He associated the New Latin word *electricus* ("of amber", from *ήλεκτρον* (elektron), the Greek word for "amber") when referring to the property of attracting small objects after being rubbed [6]. This created the English words "electric" and "electricity", first appeared in print in Thomas Browne's Pseudodoxia Epidemica of 1646 [7]. In the 18th century, Benjamin Franklin conducted extensive research in electricity [8, 9]. Alessandro Volta's battery made from alternating layers of zinc and copper, provided scientists, in 1800, a more reliable source of electrical energy than the electrostatic machines previously used [10]. The discover of unity between

electric and magnetic phenomena, **electromagnetism**, is due to Hans Christian Ørsted and André-Marie Ampère in 1819-1820. Electricity, magnetism and light, were definitively linked by James Clerk **Maxwell**, in particular in his "On Physical Lines of Force" in 1861 and 1862 [11].

With the publication "A treatise on electricity and magnetism" by Maxwell in 1893, electricity and magnetism were no longer two separate phenomena [12]. Classical electromagnetism is fully described by Maxwell, along with the Lorentz force law (that was also derived by Maxwell under the name of Equation for Electromotive Force). These same equations were the starting point for the relativity theory by Albert Einstein and are still fundamental to physics and engineering [13]. These equations show the existence of electromagnetic waves, propagating in vacuum and in matter, seemingly different phenomena like radio waves, visible light and X-rays are then understood, by interpreting them all as propagating electromagnetic waves with different frequency which is of major scientific and engineering importance even nowadays [14].

1.1.2 Definition and History of Metamaterials

From centuries scientists struggle to understand materials. The internal structure of a material sample contains so many degrees of freedom that cataloging everything in an unifying classification would be impossible. Verily, in many cases the macroscopic properties of mixtures and composite material, are very differing from those of the ingredients. Ice cream is a gross example of such a behavior: the taste is very different from the sum of tastes of ice and cream [15].

"Metamaterials" is a name for artificial materials that pays respect to this characteristic of unconventional macroscopic properties. Mainly when there are connections with electromagnetics, metamaterials are presently in a focus of intense study. Metamaterials are hard to define and classify. An inclusive defi-

nition for metamaterials that might satisfy most researchers in the field of electromagnetic materials would probably narrow down the set to those materials that simply are something else than ordinary materials. Two essential properties can be distinguish, metamaterials should exhibit properties not observed in the constituent materials and not observed in nature [16]. In the present times, the main proprieties which are not observed in nature are the effective negative permeability and permittivity, but they can be artificially achieved. This a subject of great attention on the electromagnetic community.

The start of history of metamaterials and complex media, begins with the concept of "artificial" materials in 1898, when Sir Jagadis Chunder Bose developed the first microwave experiment on twisted structures. Currently, these elements immersed in a host medium are denominated by artificial chiral medium [17, 18]. In 1914, Karl Ferdinand Lindman studied wave interaction with compilations of randomly oriented small wire helices, in order to create an artificial chiral media [19]. In 1948, Winston Kock, made lightweight microwave lenses by combination of conducting spheres, strips periodically and disks. These metamaterials, built for lower frequencies, can be designed for higher frequencies by length scaling [20]. Materials, which exhibited reversed physical characteristics were first described theoretically by Victor Veselago in 1967. When he investigated the plane wave propagation in a material which permittivity and permeability were simultaneous negative, he demonstrated that for a monochromatic uniform plane wave in this kind of media, the direction of the Poynting vector is antiparallel to the direction of phase velocity [21]. During the late 1990s, Pendry and his colleagues at Imperial College began to produce structures with these kind of properties. Pendry was interested in developing materials with negative permeability. Also, he created an array of closely spaced, thin, conducting elements, such as metal hoops [16]. In 1999, he described how he adjusted

the array's properties and he developed an array with negative permeability. This structure consisted of periodic array of split-ring resonators (SRRs) that expressed negative effective permeability over a narrow frequency band [22].

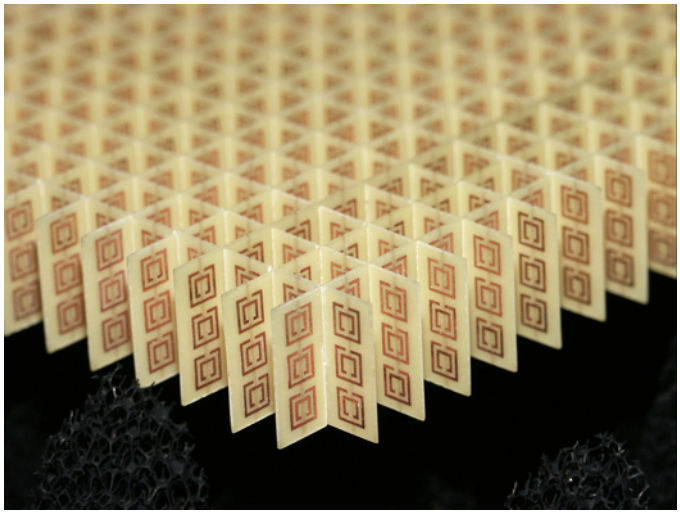

Figure 1.1: Left-handed metamaterial flat lens consisting of an array of 3 by 20 by 20 unit cells. With a unit cell width of 5 mm, this geometry shows reversed refraction and left-handed focusing properties at microwave frequencies between 10 and 11 GHz [23, 24].

This is possible if the magnetic field of incident wave is normal to the plane of the structure. Veselago medium is probably the most famous class of metamaterials in the present wave in complex electromagnetic media. Veselago medium has been known by several names, as negative-index media, negative refraction media, backward wave media (BW media), double-negative media (DNG), media with simultaneously negative permittivity and permeability and even left-handed media (LHM).

Following up on this work, in the year 2000, Smith et al. reported the experimental demonstration of functioning electromagnetic metamaterials, by horizontally stacking, periodically, split-ring resonators and thin wire structures. Later, a method was provided in 2002 to realize negative index metamaterials us-

ing artificial lumped-element loaded transmission lines in microstrip technology. At microwave frequencies, the first real invisibility cloak was realized in 2006. However, only a very small object was imperfectly hidden [20, 21, 25, 26, 27]. A core of researchers, composed mainly by Carlos Paiva, António Topa, Sérgio Matos and João Canto, contributed greatly to the study of this topic with several important works and results [28, 29, 30, 31, 32].

1.2 State of the Art

In the present days, metamaterials are synthesized by combining an array of thin metallic wires with an array of split-ring resonators. This structure provides both negative permittivity and permeability in a certain frequency bandwidth. The electromagnetic properties are only exhibited for one particular direction of propagation of the electromagnetic waves. Therefore, the magnetic field must be oriented perpendicularly to the plane of split rings until the electric field is oriented parallel to the metallic wires. The negative refraction of electromagnetic waves is being investigated in this structure and it is being prepared in laboratories. In the later years, there has been a growing interest in the theoretical and experimental study of metamaterials. But the materials were confined to small lab demonstrations because there was no way to make them in large enough quantities to demonstrate a practical device. Metamaterials that interact with visible light have previously not been made in pieces larger than hundreds of micrometers.

In 2007, one researcher [33] stated that for metamaterial applications to be realized, several goals must be achieved. Reducing energy loss, which is a major limiting factor, keep developing three-dimensional isotropic materials instead of planar structures, then finding ways to mass produce [33]. The path for mass production of metamaterials was experimentally reveled in MIT by John

Rogers and Nicholas Fang, in June 2011. With a new printing technique, these researchers can now make enough metamaterials to begin fabricating invisibility cloaks and superlenses [34].

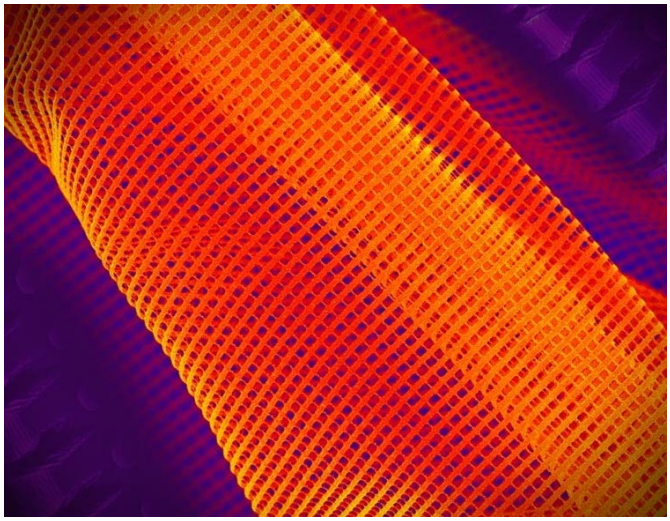

Figure 1.2: Light mesh: The large-area metamaterial is made up of a layered mesh of metals patterned on the nanoscale [34].

Rogers has developed a stamp-based printing method for generating large pieces of one of the most promising types of metamaterial, which can make near-infrared light had negative refraction index Figure 1.2. The process starts by molding a hard plastic stamp that's covered with a raised fishnet pattern. The stamp is then placed in an evaporation chamber and coated with a sacrificial layer, followed by alternating layers of the metamaterial ingredients—silver and magnesium fluoride—to form a layered mesh on the stamp. The stamp is then placed on a sheet of glass or flexible plastic and the sacrificial layer is etched away, transferring the patterned metal to the surface. For example, macroscale 2-D lenses and cloaks may be possible, and possibly solar concentrators, too. One potential application is in lenses that integrate multiple functions in single devices, for telecommunications and imaging.

1.3 Motivations and Objectives

The raise of metamaterials gave a new flame to electromagnetism. New problems and questions emerged with the physical properties of metamaterials. A large number of established physical concepts have to be re-analyzed e re-interpreted in order to fulfill the new proprieties of these materials. In the present work, we have the chance to study and strengthen various aspects of electromagnetism, with the wariness to include the new electromagnetic concepts brought by DNG media. This can be accomplished not just by studying the theory behind it, but also by analyzing simple guided structures and studying their physical electromagnetic effects.

This approach have lead to the construction of new types of microwave structures, whose applications, in mobile communications an military applications just to name a few, have attracted a lot of attention by the scientific community and also by the scientific media. Such interest comes from the fact that these metamaterials can improve a lot several communication devices, such as antennas and lens, and opened the path for invisibility cloaks. Metamaterials has also implications on lens design, since classical electrodynamics impose a resolution limit when imaging using conventional lenses. This fundamental limit, called the diffraction limit, is attributed to the finite wavelength of electromagnetic waves.

In this dissertation, about metamaterials, we shall focus on a restricted class: the DNG media. In particular, unlimited media and DNG media inserted in guides and their effects in propagation as well as study the negative refraction, taking advantage of its particular electromagnetic properties to achieve results that are not present in conventional wave guides. More specifically, study new physical phenomena that are associated with double negative media and the effects when applied to known propagation guide structures.

1.4 Organization and Structure of the Dissertation

This dissertation is composed by five chapters. The first one is an introduction so the reader can situate the present work in the subject. It starts with an overview of the historical background, where the main researchers and publications are referred. The state of the art of complex media is revealed in order to see the evolution through history until the present day. Motivations and objectives of this dissertation are explained, followed by it's organization and structure as well as the original contributions.

In the second chapter the electromagnetic proprieties of DNG metamaterials are studied. Firstly, a media classification is done according to the real part of permittivity and permeability, followed by the characterization of a medium where both values are negative. This leads to the appearance the backward waves that are analyzed as well as negative refraction. Since this complex materials reveals fundamental problems when the dispersion is not taken in to account, a dispersive study is done using mainly the Lorentz Dispersive Model. This study also allows us to see the difference between phase and group velocities in DNG media or in DPS media.

In the the third chapter guided wave propagation with DNG media is studied for a DPS-DNG interface. After modal analysis, numerical simulations are done to both non dispersive and dispersive model, using the Lorentz Dispersive Model, being the results (permeability, permittivity and refractive index) compared and interpreted. The TE and the TM modes are studied in both cases, computing dispersion relations and attenuation constants.

For a more practical view of the DNG-DPS interface, a problem is formulated assuring that resonances of both the permeability and permittivity are close

enough, which is one of the main problems when creating metamaterials. Some simulations are obtained for various values of filling factor, a media classification in frequency is done, and the existence of TM and TE modes is analyzed.

In the the fourth chapter another guided wave structure, recurring to DNG media, is studied. In this case, we study a DNG slab which outer medium is an unlimited DPS media. First, the modal equations are calculated, applying boundary conditions to the tangential field components and doing relations between the normalized wave numbers. This results in modal equations for the TE odd mode and TM even mode. A DPS medium only allows modal solutions with real transverse wave numbers providing slow modes. Solutions with imaginary transverse wave numbers, when using a dielectric DNG slab, may also be found. This result provides super-slow modes, where the phase velocity is lower than the speed of light in the medium, while for conventional slow modes, the phase velocity is limited by a lower bound.

Finally, in the fifth and last chapter, the main conclusions are gathered and some future work is suggested as well as some potential applications for complex media.

1.5 Original Contributions

Metamaterials are a topic that has rising interest among electromagnetics research community. Many publications and studies were made for this topic of discussion, most of the are scattered. The main contribution of this dissertation it to collect and gather these studies and problems in such a way that can be useful for future researchers in this field of interest. The studies presented here, contain an introduction to the electromagnetics of the DNG media and guided electromagnetic wave propagation in planar structures containing both double

positive media (DPS) and DNG materials. A less theoretical problem is also object of analysis.

Chapter 2

Electromagnetics of DNG Metamaterials

In this chapter, the propagation properties of double negative (DNG) metamaterials are addressed. Plane wave propagation is studied in an isotropic and unlimited DNG medium, using Maxwell's equations. Negative refraction and anti-parallel Poynting vector are also studied.

2.1 Media Classification

In the present work, we consider a **double negative** (**DNG**) metamaterial being characterized by two constitutive parameters, the permittivity, ε, and the permeability, μ. These parameters can usually be described by the following relations,

$$\varepsilon = \varepsilon' + i\varepsilon'' \tag{2.1}$$

with $\varepsilon', \varepsilon'' \ \epsilon \ \Re$, and

$$\mu = \mu' + i\mu'' \tag{2.2}$$

with $\mu', \mu'' \ \epsilon \ \Re$.

Assuming that a medium can be classified by the real part of both ε and μ, the DNG classification is due to

$$\begin{cases} \varepsilon' = \Re(\varepsilon) < 0 \\ \\ \mu' = \Re(\mu) < 0 \end{cases} \tag{2.3}$$

In the same way, we classify a **double positive medium** (**DPS**) as

$$\begin{cases} \varepsilon' = \Re(\varepsilon) > 0 \\ \\ \mu' = \Re(\mu) > 0 \end{cases} \tag{2.4}$$

A **simple negative medium** (**SNG**), where $\varepsilon'(\omega)\mu'(\omega) < 0$, can be divided in two. An **epsilon negative medium** (**ENG**) with

$$\begin{cases} \varepsilon' = \Re(\varepsilon) < 0 \\ \\ \mu' = \Re(\mu) > 0 \end{cases} \tag{2.5}$$

And a **mu negative medium** (**MNG**) with

$$\begin{cases} \varepsilon' = \Re(\varepsilon) > 0 \\ \\ \mu' = \Re(\mu) < 0 \end{cases} \tag{2.6}$$

In Figure2.1 [36] we have the materials classified according to the real part of ε and μ.

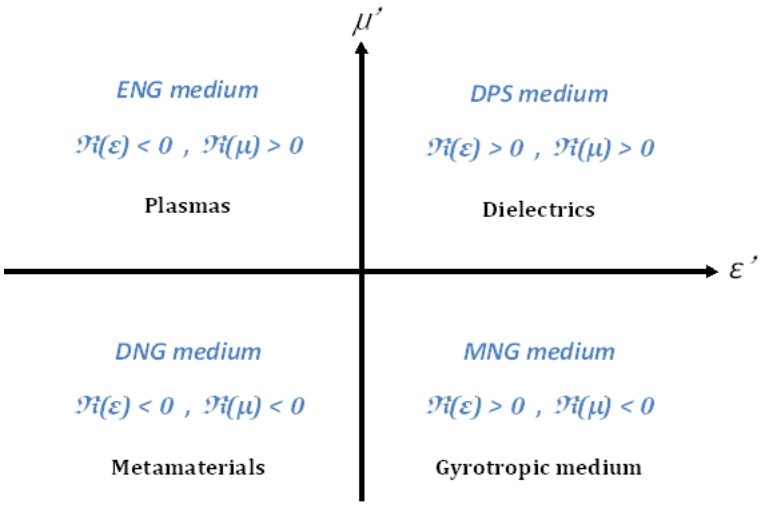

Figure 2.1: Media classification by permeability and permittivity

The constitutive relations, in the frequency domain, can be written by

$$\begin{cases} \varepsilon(\omega) = 1 + \chi_e(\omega) \\ \\ \mu(\omega) = 1 + \chi_m(\omega) \end{cases} \rightarrow \begin{cases} \mathbf{D} = \varepsilon_0 \varepsilon(\omega)\mathbf{E} \\ \\ \mathbf{B} = \mu_0 \mu(\omega)\mathbf{H} \end{cases} \tag{2.7}$$

Where $\chi_e(\omega)$ is electric susceptibility and $\chi_m(\omega)$ the magnetic susceptibility. Considering the electric field polarized along x-axis and the electromagnetic wave propagating in the z-axis, we can write the electric and magnetic fields as follows

$$\begin{cases} \mathbf{E} = \widehat{x} E_0 \exp[i(\mathbf{k}z - \omega t)] \\ \\ \mathbf{H} = \widehat{y} H_0 \exp[i(\mathbf{k}z - \omega t)] \end{cases} \rightarrow \begin{cases} \mathbf{E}_0 = \widehat{x}\Re(E_0) \\ \\ \mathbf{H}_0 = \widehat{y}\Re(H_0) \end{cases} \tag{2.8}$$

The vacuum wave number, k_0, is given by

$$k_0 = \omega\sqrt{\varepsilon_0\mu_0} = \frac{\omega}{c} \tag{2.9}$$

Where the wave number, k, relates with the k_0 through the refractive index, $n = n(\omega)$, expressed as

$$\mathbf{k} = \hat{\mathbf{z}}k \rightarrow k = k(\omega) = n(\omega)k_0 = n(\omega)\frac{\omega}{c} \tag{2.10}$$

The wave impedance in the present medium is given by

$$\eta = \frac{E_0}{H_0} \tag{2.11}$$

Where E_0 is the electric field intensity and H_0 the magnetic field intensity.

From the Maxwell's equations, applied to the plane waves propagating in the isotropic and unlimited medium, we get

$$\mathbf{k}\cdot\mathbf{E} = \mathbf{k}\cdot\mathbf{H} = 0, \begin{cases} \mathbf{k}\times\mathbf{E} = \omega\mu_0\mu\mathbf{H} \\ \\ \mathbf{k}\times\mathbf{H} = -\omega\varepsilon_0\varepsilon\mathbf{E} \end{cases} \tag{2.12}$$

$$\therefore \begin{pmatrix} k & -\omega\mu_0\mu \\ -\omega\varepsilon_0\varepsilon & k \end{pmatrix} \begin{pmatrix} E_0 \\ H_0 \end{pmatrix} = \begin{pmatrix} 0 \\ 0 \end{pmatrix} \tag{2.13}$$

With $\mathbf{E}$ being the electric field vector and $\mathbf{H}$ the magnetic field vector. With this, we have

$$k^2 = \omega^2\varepsilon_0\mu_0\varepsilon\mu = \left(\frac{\omega}{c}\right)^2\varepsilon\mu \tag{2.14}$$

With

$$k = n\,k_0 \tag{2.15}$$

Where the refractive index is expressed as

$$n = \sqrt{\varepsilon\mu} \tag{2.16}$$

and

$$\eta = \frac{k}{\omega\varepsilon_0\varepsilon} = \frac{\omega\mu_0\mu}{k} = \zeta\eta_0 \tag{2.17}$$

where

$$\eta_0 = \sqrt{\frac{\mu_0}{\varepsilon_0}} \tag{2.18}$$

Leading us to

$$\zeta = \frac{\eta}{\eta_0} = \sqrt{\frac{\mu}{\varepsilon}} \tag{2.19}$$

With η_0 being the vacuum wave impedance. Note that the normalized wave impedance can be re-written to

$$\zeta = \frac{n}{\varepsilon} = \frac{\mu}{n} \tag{2.20}$$

In these conditions,

$$\mathbf{k} = k\hat{\mathbf{z}} = (n\,k_0) \rightarrow \begin{cases} \mathbf{E} = \hat{\mathbf{x}} E_0 \exp(i\,n\,k_0 z) \\ \\ \mathbf{H} = \hat{\mathbf{y}} \frac{E_0}{\zeta\eta_0} \exp(i\,n\,k_0 z) \end{cases} \tag{2.21}$$

The average value of the Poynting vector for the frequency ω will be

$$\mathbf{S}_\omega = \frac{1}{2}\Re\left(\mathbf{E}\times\mathbf{H}^*\right) = \hat{\mathbf{z}}\frac{1}{2}\Re\left(E_0 H_0^*\right) = \hat{\mathbf{z}}\frac{|E_0|^2}{2\eta_0}\Re\left(\frac{1}{\zeta}\right)\exp\left[-2\Im(k)z\right] \tag{2.22}$$

As shown, the condition for the medium to be passive is

$$\Im(k) = k'' > 0 \tag{2.23}$$

for an electromagnetic wave that propagates through the positive z axis.

The polarization never responds instantaneously to an applied field. This causes dielectric loss which are expressed by permittivity and permeability that are both complex and frequency dependent. Material, both natural and artificial, are not perfect insulators either, they have non-zero direct current conductivity [35]. Considering this, we can define a complex refractive index as

$$n = n' + i\,n'' \tag{2.24}$$

with $n' = \Re(n)$ and $n'' = \Im(n)$.

We can now write the complex amplitude equations for both the electric and the magnetic field using (2.24)

$$\begin{cases} \mathbf{E} = \hat{\mathbf{x}}E_0\exp(i\,n\,k_0 z) = \hat{\mathbf{x}}E_0\exp(-n''\,k_0 z)\exp(i\,n'k_0 z) \\ \\ \mathbf{H} = \hat{\mathbf{y}}\frac{E_0}{\zeta\eta_0}\exp(i\,n\,k_0 z) = \hat{\mathbf{y}}\frac{E_0}{\zeta\eta_0}\exp(-n''\,k_0 z)\exp(i\,n'k_0 z) \end{cases} \tag{2.25}$$

We can also call n'' the extinction coefficient a represent it by κ. Once again the passive medium must have

$$\Im(n) = n'' = \kappa > 0 \tag{2.26}$$

since, otherwise we wouldn't have the condition of passive medium for an electromagnetic wave whose energy propagates through the positive z axis,

$$\lim_{z\to\infty} |\mathbf{E}| \leq |E_0| \tag{2.27}$$

2.2 Backward Waves

As we will verify in the following section, in a DNG medium, the trihedral $[\mathbf{E}_0, \mathbf{H}_0, \Re(\mathbf{k})]$ is left handed. In the other way, as expected, the trihedral for a DPS medium, $[\mathbf{E}_0, \mathbf{H}_0, \Re(\mathbf{k})]$ is right handed. But, for both a DPS or a DNG medium, the trihedral $[\mathbf{E}_0, \mathbf{H}_0, \mathbf{S}_\omega]$ is always right handed.

From the Maxwell's equations, in the differential form, we can easily assimilated the left hand rule [21]

$$\nabla \times \mathbf{E} = -\frac{\partial \mathbf{B}}{\partial t} \tag{2.28}$$

$$\nabla \times \mathbf{H} = \frac{\partial \mathbf{D}}{\partial t} \tag{2.29}$$

to describe the response of the medium to the applied fields, we have the two constitutive relations,

$$\mathbf{B} = \mu_0 \mu \mathbf{H} \tag{2.30}$$

$$\mathbf{D} = \varepsilon_0 \varepsilon \mathbf{E} \tag{2.31}$$

In the time harmonic regime, the following relations between operators can be derived

$$\frac{\partial}{\partial t} \rightarrow -i\,\omega \tag{2.32}$$

and

$$\nabla \rightarrow i\,\mathbf{k} \tag{2.33}$$

In order to calculate the sign of the Poynting vector, $\mathbf{S}$, and of the wave vector, $\mathbf{k}$, we use the following relations for the spacial orientation of the electric and magnetic field vectors, $\mathbf{E}$ and $\mathbf{H}$,

$$\mathbf{k} \times \mathbf{E} = \omega \mu_0 \mu \mathbf{H} \tag{2.34}$$

$$\mathbf{k} \times \mathbf{H} = -\omega \varepsilon_0 \varepsilon \mathbf{E} \tag{2.35}$$

As shown on the following figure,

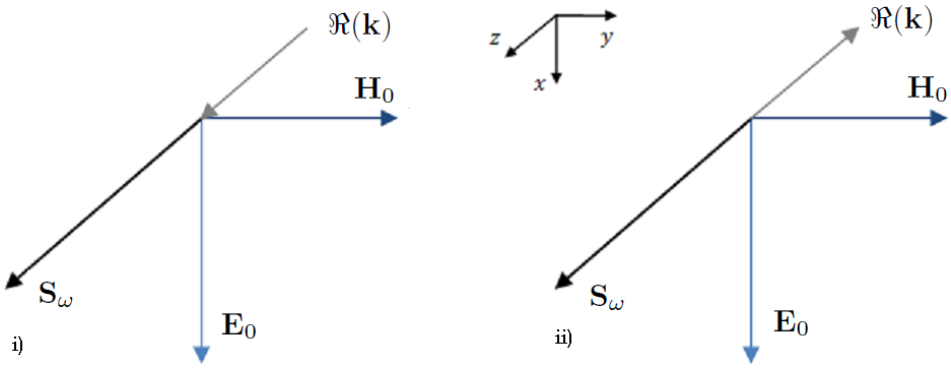

Figure 2.2: Trihedral vectores for the i) DPS and ii) DNG media.

From Figure 2.2 we can see that in the DPS medium, both vectors, $\mathbf{k}$ and $\mathbf{S}$,

have the same direction. Creating a **forward wave**, meaning that the electromagnetic wave and the electromagnetic energy have the same direction. Moreover we can see that the vectors **k** and **S** have opposite orientation in the DNG medium. This results in a **backward wave**, which means that the electromagnetic wave and the electromagnetic energy have opposite directions.

It's important to note that the phase velocity of this electromagnetic wave is given by

$$\begin{cases} k = n\,k_0 \\ k = k' + i\,k'' \\ n = n' + i\,n'' \end{cases} \rightarrow \mathbf{v}_p = \frac{\omega}{\Re(\mathbf{k})} = \frac{\omega}{k_0 \Re(\mathbf{n})} = \frac{c}{\Re(\mathbf{n})} = \frac{c}{\mathbf{n}'} \tag{2.36}$$

In order to obtain valid roots to (2.16) and (2.19), since in general $\varepsilon, \mu \in \mathbb{C}$, we can re-write (2.22), for a DPS or DNG media, as

$$\Re\left(\frac{1}{\zeta}\right) = \Re\left(\frac{1}{\mu}\right) = \Re\left(\frac{n' + i\,n''}{\mu' + i\,\mu''}\right) = \frac{n'\mu' + n''\mu''}{(\mu')^2 + (\mu'')^2} \tag{2.37}$$

Since this is a passive medium, we have $\varepsilon'' > 0$, $\mu'' > 0$ and $n'' > 0$. Furthermore, being a DNG medium, we also have $\varepsilon' < 0$ and $\mu' < 0$ and, as we shall see later, $n' > 0$. Knowing this, we must verify the following condition

$$\frac{n'\mu' + n''\mu''}{(\mu')^2 + (\mu'')^2} > 0 \Rightarrow \hat{\mathbf{z}} \cdot \mathbf{S}_\omega > 0 \tag{2.38}$$

The same result obtained in (2.38), is applied to the DPS medium since $\varepsilon' > 0$ and $\mu' > 0$, when multiplied, have the same signal than $\varepsilon' < 0$ than $\mu' < 0$.

We will now study the permittivity in the complex plan using polar coordinates, but the same study can be applied to the permeability,

$$\begin{cases} \varepsilon = \varepsilon' + i\,\varepsilon'' = \rho_\varepsilon \exp(i\,\theta_\varepsilon) \\ \\ \mu = \mu' + i\,\mu'' = \rho_\mu \exp(i\,\theta_\mu) \end{cases} \tag{2.39}$$

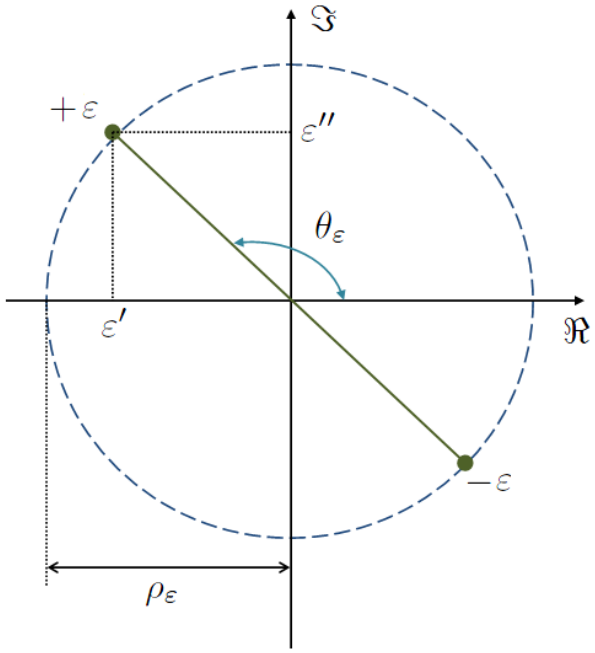

Figure 2.3: Electric permittivity in the complex plan.

Since

$$cos(\theta_\varepsilon) = \pm \frac{1}{\sqrt{1 + \tan^2(\theta_\varepsilon)}} \tag{2.40}$$

we get

$$\begin{cases} \rho_\varepsilon = \sqrt{(\varepsilon')^2 + (\varepsilon'')^2} = |\varepsilon'| \sqrt{1 + \left(\frac{\varepsilon''}{\varepsilon'}\right)^2} \\ \\ \cos(\theta_\varepsilon) = sgn(\varepsilon') \dfrac{1}{\sqrt{1 + \left(\frac{\varepsilon''}{\varepsilon'}\right)}} = sgn(\varepsilon') \dfrac{|\varepsilon'|}{\sqrt{(\varepsilon')^2 + (\varepsilon'')^2}} \end{cases} \tag{2.41}$$

and therefore

$$\varepsilon' = \rho_\varepsilon \cos(\theta_\varepsilon) < 0 \rightarrow \cos(\theta_\varepsilon) = \frac{\varepsilon'}{\sqrt{(\varepsilon')^2 + (\varepsilon'')^2}} < 0 \tag{2.42}$$

Using once again the polar coordinates, n_ε is represented in the following figure

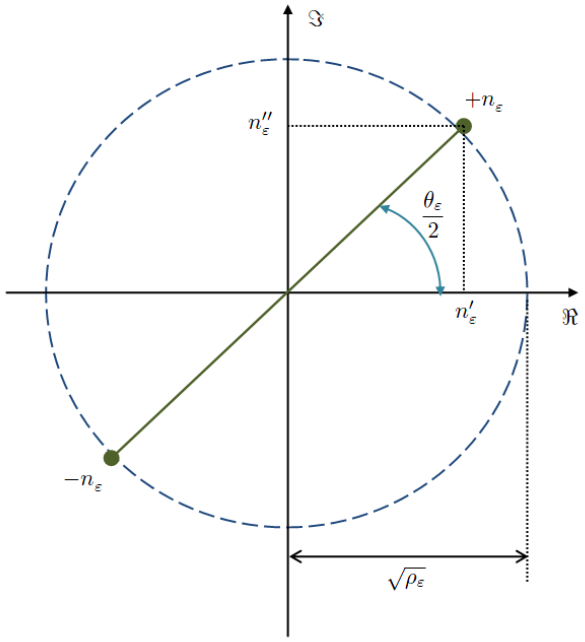

Figure 2.4: $n_\varepsilon$in the complex plan.

For a DNG medium, we got $\varepsilon' < 0$, meaning that the permittivity angle is confined by $\pi \geq \theta_\varepsilon \geq \pi/2$ but then $\pi/2 \geq \theta_\varepsilon/2 \geq \pi/4$, where

$$n_\varepsilon = n'_\varepsilon + i\, n''_\varepsilon = \sqrt{\varepsilon} = \rho_\varepsilon^{1/2} \exp\left(i\frac{\theta_\varepsilon}{2}\right) \tag{2.43}$$

$$\therefore n_\varepsilon = i(n''_\varepsilon - i\, n''_\varepsilon) = i\, \rho_\varepsilon^{1/2} \left[\sin\left(\frac{\theta_\varepsilon}{2}\right) - i\left(\frac{\theta_\varepsilon}{2}\right)\right] \tag{2.44}$$

Where, given that

$$\begin{cases} \cos\left(\frac{\theta_\varepsilon}{2}\right) = \sqrt{\frac{1+\cos(\theta_\varepsilon)}{2}} \\ \\ \sin\left(\frac{\theta_\varepsilon}{2}\right) = \sqrt{\frac{1-\cos(\theta_\varepsilon)}{2}} \end{cases} \tag{2.45}$$

We are expected to have

$$\begin{cases} \cos\left(\frac{\theta_\varepsilon}{2}\right) = \frac{1}{\sqrt{2}} \left[1 + \frac{\varepsilon'}{\sqrt{(\varepsilon')^2 + (\varepsilon'')^2}}\right]^{1/2} > 0 \\ \\ \sin\left(\frac{\theta_\varepsilon}{2}\right) = \frac{1}{\sqrt{2}} \left[1 - \frac{\varepsilon'}{\sqrt{(\varepsilon')^2 + (\varepsilon'')^2}}\right]^{1/2} > 0 \end{cases} \tag{2.46}$$

Since must chose the positive root to obtain $n'_\varepsilon \geq 0$ and $n''_\varepsilon > 0$, we get

$$n'_\varepsilon = \sqrt{\frac{|\varepsilon'|}{2}} \left[1 + \left(\frac{\varepsilon''}{\varepsilon'}\right)^2\right]^{\frac{1}{4}} \left[1 + \frac{sgn(\varepsilon')}{\sqrt{1 + \left(\frac{\varepsilon''}{\varepsilon'}\right)^2}}\right]^{\frac{1}{2}} \tag{2.47}$$

and

$$n'_\varepsilon = \sqrt{\frac{|\varepsilon'|}{2}} \left[1 + \left(\frac{\varepsilon''}{\varepsilon'}\right)^2\right]^{\frac{1}{4}} \left[1 - \frac{sgn(\varepsilon')}{\sqrt{1 + \left(\frac{\varepsilon''}{\varepsilon'}\right)^2}}\right]^{\frac{1}{2}} \tag{2.48}$$

Due to the fact that a DNG medium has $sgn(\varepsilon') = -1$, we can say $n''_\varepsilon > n'_\varepsilon$. In the limit case, were the losses are not considered, $\varepsilon'' = 0$, we have

$$sgn(\varepsilon') = -1 \rightarrow \begin{cases} n'_\varepsilon = 0 \\ \\ \\ n''_\varepsilon = |\varepsilon'|^{1/2} \end{cases} \rightarrow n_\varepsilon = i\,|\varepsilon'|^{1/2} \tag{2.49}$$

similarly we get

$$n'_\mu = \sqrt{\frac{|\mu'|}{2}} \left[1 + \left(\frac{\mu''}{\mu'}\right)^2\right]^{\frac{1}{4}} \left[1 + \frac{sgn(\mu')}{\sqrt{1 + \left(\frac{\mu''}{\mu'}\right)^2}}\right]^{\frac{1}{2}} \tag{2.50}$$

$$n'_\mu = \sqrt{\frac{|\mu'|}{2}} \left[1 + \left(\frac{\mu''}{\mu'}\right)^2\right]^{\frac{1}{4}} \left[1 - \frac{sgn(\mu')}{\sqrt{1 + \left(\frac{\mu''}{\mu'}\right)^2}}\right]^{\frac{1}{2}} \tag{2.51}$$

Once again, due to the fact that this is a DNG medium, $sgn(\mu') = -1$, we can say $n''_\mu > n'_\mu$. In the limit case, where the losses are not considered, $\mu'' = 0$, we have

$$sgn(\mu') = -1 \rightarrow \begin{cases} n'_\mu = 0 \\ \\ \\ n''_\mu = |\mu'|^{1/2} \end{cases} \rightarrow n_\mu = i\,|\mu'|^{1/2} \tag{2.52}$$

So, in the limit case where there aren't loses, $\varepsilon'' = \mu'' = 0$, leads, according to (2.49) and (2.52), to the negative value

$$\text{DNG medium} \rightarrow n = n_\varepsilon n_\mu = (i\,n''_\varepsilon)(i\,n''_\mu) = -\,|\varepsilon'|^{1/2}\,|\mu'|^{1/2} < 0 \tag{2.53}$$

In the general case, the medium refraction index is [37]

$$
\begin{aligned}
n = n' + i\,n'' &= n_\varepsilon n_\mu \\
&= (n'_\varepsilon + i\,n''_\varepsilon)(n'_\mu + i\,n''_\mu) \\
&= [i(n''_\varepsilon - i\,n'_\varepsilon)][i(n''_\mu - i\,n'_\mu)] \\
&= -(n''_\varepsilon - i\,n'_\varepsilon)(n''_\mu - i\,n'_\mu) \\
&= -\left[(n''_\varepsilon n''_\mu - n'_\varepsilon n'_\mu) - i(n'_\varepsilon n''_\mu + n'_\mu n''_\varepsilon)\right]
\end{aligned}
$$

$$
\therefore \text{DNG medium} \rightarrow \begin{cases} n' = -(n''_\varepsilon n''_\mu - n'_\varepsilon n'_\mu) < 0 \\ \\ n'' = n'_\varepsilon n''_\mu + n'_\mu n''_\varepsilon > 0 \end{cases} \tag{2.54}
$$

From

$$
\text{DNG medium} \rightarrow \begin{cases} \varepsilon' < 0 \\ \\ \mu' < 0 \end{cases} \rightarrow n = \rho_n \exp(i\theta_n) = \rho_\varepsilon^{1/2} \rho_\mu^{1/2} \exp\left(i\tfrac{\theta_\varepsilon + \theta_\mu}{2}\right) \tag{2.55}
$$

having $\pi \geq \theta_n > \pi/2$ hence one can infer that

$$
k = k' + i\,k'' = n\,k_0 = (n' + i\,n'')\frac{\omega}{c} \tag{2.56}
$$

$$
\text{DNG medium} \rightarrow \Re(k) = k' = \frac{n'\omega}{c} < 0 \rightarrow \mathbf{S}_\omega \cdot \Re(\mathbf{k}) < 0 \tag{2.57}
$$

With (2.57) we can see that the real part of $\mathbf{k}$ and the Poynting vector, $\mathbf{S}_\varepsilon$,

have opposite sign, which corresponds to backward waves, the same conclusion obtained with the trihedral vectors.

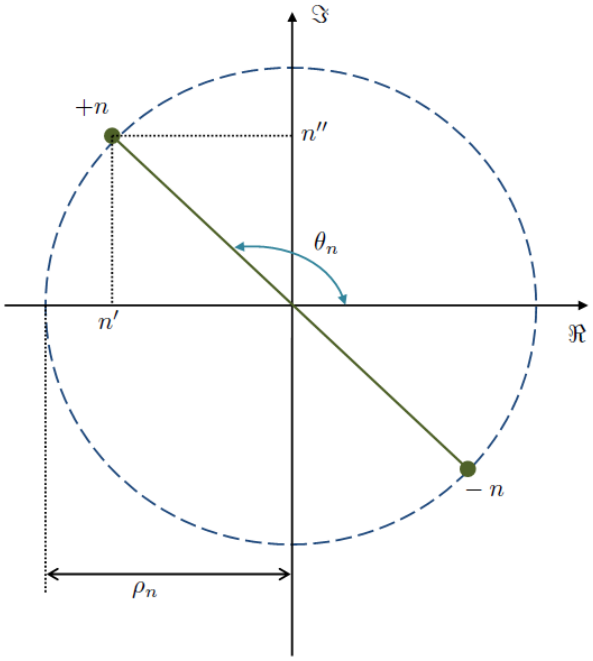

Figure 2.5: Refractive index in the complex plan.

Once the complex value of n is determined, the complex value of ζ is also unequivocally determined through (2.20). We get

$$\zeta = \frac{n}{\varepsilon} = \frac{n' + i\,n''}{\varepsilon' + i\,\varepsilon''} = \frac{(n'\varepsilon' + n''\varepsilon'') + i(n''\varepsilon' - n'\varepsilon'')}{(\varepsilon')^2 + (\varepsilon'')^2} \tag{2.58}$$

In the case where the loses are disregarded, $\varepsilon'' = n'' = 0$, we got

$$\zeta = \frac{n}{\varepsilon'} = \sqrt{\frac{\mu'}{\varepsilon'}} = \frac{|\mu'|^{1/2}}{|\varepsilon'|^{1/2}} \tag{2.59}$$

If we had chosen the other possible solution for n, $\Im(n) = n'' = 0$, we would get

$$\text{DNG medium} \rightarrow \begin{cases} n' = (n''_{\varepsilon} n''_{\mu} - n'_{\varepsilon} n'_{\mu}) > 0 \\ \\ n'' = -(n'_{\varepsilon} n''_{\mu} + n'_{\mu} n''_{\varepsilon}) < 0 \end{cases} \tag{2.60}$$

Which, in the limit case, where there aren't any loses, we would get a positive refraction index and non negative like in (2.53). Therefore, with $n'_{\varepsilon} = n'_{\mu} = 0$, we get

$$\text{DNG medium} \rightarrow \begin{cases} n = n''_{\varepsilon} n''_{\mu} = |\varepsilon'|^{1/2} |\mu'|^{1/2} => 0 \\ \\ \zeta = \frac{n}{\varepsilon'} = -\sqrt{\frac{\mu'}{\varepsilon'}} = -\frac{|\mu'|^{1/2}}{|\varepsilon'|^{1/2}} < 0 \end{cases} \tag{2.61}$$

The main difference between the two solutions of n, the solution we chose equivalent to $\Im(n) > 0$ and the solution corresponding to $\Im(n) < 0$, is the one we can get from (2.22). The first solution corresponds to a direction of power flux in the positive direction $(+z)$. The second solutions corresponds, as expected, to a direction of power flux in the negative direction $(-z)$. However, whatever the solution chosen, we can always verify that

$$\mathbf{S}_{\omega} \cdot \Re(\mathbf{k}) < 0 \tag{2.62}$$

This is due to the power flux being diametrically opposed to the direction in which the amplitude of the electric field increases.

Note that the DPS medium case, with $\varepsilon' > 0$ and $\mu' > 0$, corresponds to the normal case where $\pi/2 > \theta_{\varepsilon} \geq 0$ and $\pi/2 > \theta_{\mu} \geq 0$, whereby we have $n'_{\varepsilon} > n''_{\varepsilon}$ and $n'_{\mu} > n''_{\mu}$. This way, the expression (2.55) is still valid. However, for a DPS medium, we have $\pi/2 > \theta_n \geq 0$, so

$$\mathbf{S}_\omega \cdot \Re(\mathbf{k}) > 0 \tag{2.63}$$

Meaning that the power flux has diametrically the direction in which the amplitude of the electric field increases. When we neglect loses, $n''_\varepsilon = n''_\mu = 0$, we got

$$\text{DPS medium} \rightarrow n = n_\varepsilon n_\mu = n'_\varepsilon n'_\mu = |\varepsilon'|^{1/2} |\mu'|^{1/2} > 0 \tag{2.64}$$

Since (2.63) is verified for both the lossy and the lossless media, due to the positive real part of the refraction index, this suggests forward electromagnetic waves.

2.3 Dispersion

From the laws of Electromagnetism, we know that for a certain isotropic medium, defined by ε and μ,

$$\langle W_e \rangle = \frac{1}{4} \varepsilon \varepsilon_0 \overline{\mathbf{E}} \cdot \overline{\mathbf{E}}^* \tag{2.65}$$

$$\langle W_m \rangle = \frac{1}{4} \mu \mu_0 \overline{\mathbf{H}} \cdot \overline{\mathbf{H}}^* \tag{2.66}$$

Where $\langle W_e \rangle$ is the time-average electric density and $\langle W_m \rangle$ the time average magnetic density. If both ε and μ are negative, like in DNG media, we have fundamental problems since we can't have negative energy density. This proves that a DNG medium is necessarily dispersive due to the definition of electromagnetic energy. Therefore both equations, (2.65) and (2.66), are invalid and need to be corrected to a lossless dispersive media [38],

$$\langle W_e \rangle = \int_{-\infty}^{t} \frac{\partial \mathbf{D}}{\partial t'} \mathbf{E} dt' \tag{2.67}$$

$$\langle W_m \rangle = \int_{-\infty}^{t} \frac{\partial \mathbf{B}}{\partial t'} \mathbf{H} dt' \tag{2.68}$$

Both the electric and the magnetic fields are almost monochromatic, with $\mathbf{E}(t) = \overline{\mathbf{E}}\exp(-vt)$ and $\mathbf{H}(t) = \overline{\mathbf{H}}\exp(-vt)$ respectively, where the period variation is very slow $T = 2\pi/\omega$, meaning that $v << \omega$.

2.3.1 Group Velocity and Phase Velocity

The expression for the time-average energy density of a monochromatic plane wave is defined by:

$$\langle W \rangle = \frac{1}{4}\left[\varepsilon_0 \frac{\partial(\omega\,\varepsilon)}{\partial\omega}\left|\mathbf{E}\right|^2 + \mu_0 \frac{\partial(\omega\,\mu)}{\partial\omega}\left|\mathbf{H}\right|^2\right] \tag{2.69}$$

If we consider

$$\mathcal{A} = \mu\varepsilon + \omega\mu\frac{\partial(\omega\,\varepsilon)}{\partial\omega} + \mu\varepsilon + \omega\varepsilon\frac{\partial(\omega\,\mu)}{\partial\omega} = 2\mu\varepsilon + \omega\left[\mu\frac{\partial(\omega\varepsilon)}{\partial\omega} + \varepsilon\frac{\partial(\omega\mu)}{\partial\omega}\right] \tag{2.70}$$

As seen in the previous section, in a DNG medium we have $\mu < 0$ and $\varepsilon < 0$, leading us to $\mathcal{A} < 0$. From (2.14) and (2.20) we have,

$$\mathbf{k}^2 = \omega^2\mu_0\mu\varepsilon_0\varepsilon \tag{2.71}$$

Applying the first derivative in order of the ω to $\mathbf{k}^2$, we get

$$\frac{\partial(\mathbf{k}^2)}{\partial\omega} = \mu_0\varepsilon_0\frac{\partial\left(\omega^2\mu\varepsilon\right)}{\partial\omega} = \mu_0\varepsilon_0\omega\left[2\varepsilon\mu + \omega\mu\frac{\partial(\omega\varepsilon)}{\partial\omega} + \omega\varepsilon\frac{\partial(\omega\mu)}{\partial\omega}\right] = \mu_0\varepsilon_0\omega\mathcal{A} \tag{2.72}$$

From (2.9) and (2.15) we obtain,

$$\mathbf{k} = nk_0 = n\frac{\omega}{c} \tag{2.73}$$

Which enables us to write (2.72) as

$$\frac{\partial(\mathbf{k}^2)}{\partial\omega} = 2\mathbf{k}\frac{\partial(\mathbf{k})}{\partial\omega} = 2nk_0\frac{\partial(\mathbf{k})}{\partial\omega} = 2\mathbf{n}\frac{\omega}{c}\frac{\partial(\mathbf{k})}{\partial\omega} \tag{2.74}$$

The **Phase Velocity**, $\mathbf{v}_p$, is given by

$$\mathbf{v}_p = \frac{\omega}{\Re(\mathbf{k})} = \frac{\omega}{k_0\Re(\mathbf{n})} = \frac{c}{\mathbf{n}'} \tag{2.75}$$

and the **Group Velocity**, $\mathbf{v}_g$, is given by

$$\mathbf{v}_g = \frac{\partial\omega}{\partial\mathbf{k}} \tag{2.76}$$

Replacing (2.75) and (2.76) on (2.74) , we have

$$\frac{\partial(\mathbf{k}^2)}{\partial\omega} = 2\omega\frac{1}{\mathbf{v}_p}\frac{1}{\mathbf{v}_g} \tag{2.77}$$

For a lossy DNG medium, $\varepsilon < 0$ and $\mu < 0$, we have $\mathcal{A} < 0$ which implies that

$$\frac{\partial(\mathbf{k}^2)}{\partial\omega} < 0 \tag{2.78}$$

Since we cannot have negative energy density, we must conclude that v_G and v_P have different signs (and opposite directions).

For a non-dispersive media, one has $v_G = v_P$. On the DNG media, that has to be dispersive, one can prove that both group velocity and phase velocity, not only have different signs, but also has different values. Applying the first derivative in order of the ω on (2.73), we get

$$\frac{\partial(\mathbf{k})}{\partial\omega} = \frac{\partial(\omega\mathbf{n})}{\partial\omega}\frac{1}{c} = \frac{1}{c}\left(n + \omega\frac{\partial\mathbf{n}}{\partial\omega}\right) \tag{2.79}$$

Applying (2.75) and (2.76) on (2.79)

$$\frac{1}{\mathbf{v}_g} = \frac{1}{\mathbf{v}_p} + \frac{1}{c}\omega\frac{\partial\mathbf{n}}{\partial\omega} \tag{2.80}$$

Due to last parcel, the group velocity is only equal to the phase velocity when the refraction index is frequency independent.

2.3.2 Lorentz Dispersive Model

In this section we will analyze the fundamental issue for the DNG medium, the **dispersion** (in the time domain). Due to the definition of electromagnetic energy density, a DNG medium has to be necessarily dispersive.

In the work, we will use the **Lorentz Dispersive Model** (LDM),

$$\begin{cases} \varepsilon(\omega) = 1 + \frac{\omega_{pe}^2}{\omega_{0e}^2 - i\omega\Gamma_e - \omega^2} \\ \\ \mu(\omega) = 1 + \frac{\omega_{pm}^2}{\omega_{0m}^2 - i\omega\Gamma_m - \omega^2} \end{cases} \tag{2.81}$$

where $\omega_{0e,m}$ represent resonance frequency, $\omega_{pe,m}$ are values for the plasma frequencies and $\Gamma_{e,m}$ collision frequencies (i.e. losses). In the LDM, we can find a frequency range $[\omega_{1e,m}, \omega_{2e,m}]$ where the parameters $\varepsilon(\omega)$ and $\mu(\omega)$ have a negative real part.

$$\begin{cases} \begin{cases} \omega_{1e} = \omega_\varepsilon \\ \omega_{2e} = \omega_b \end{cases} \\ \\ \begin{cases} \omega_{1m} = \omega_a \\ \omega_{2m} = \omega_\mu \end{cases} \end{cases} \rightarrow \begin{array}{l} \Re(\varepsilon) < 0 \rightarrow [\omega_\varepsilon, \omega_b] \\ \Re(\mu) < 0 \rightarrow [\omega_a, \omega_\mu] \end{array} \tag{2.82}$$

In order to simplify the above expressions, we remove the index e, that corresponds to the relative dielectric permittivity, and m, that corresponds to the relative magnetic permeability. This simplifications leads us to

$$\begin{cases} 2\omega_1^2 = \left(2\omega_0^2 + \omega_p^2 - \Gamma^2\right) - \sqrt{\omega_p^4 + \Gamma^4 - 2\Gamma\omega_p^2 - 4\Gamma^2\omega_0^2} \\ \\ 2\omega_2^2 = \left(2\omega_0^2 + \omega_p^2 - \Gamma^2\right) + \sqrt{\omega_p^4 + \Gamma^4 - 2\Gamma\omega_p^2 - 4\Gamma^2\omega_0^2} \end{cases} \tag{2.83}$$

If we neglect the losses, $\Gamma = 0$, we get

$$\Gamma = 0 \rightarrow \begin{cases} \omega_1 = \omega_0 \\ \omega_2 = \sqrt{\omega_0^2 + \omega_p^2} \end{cases} \tag{2.84}$$

A media will only be considered DNG if confined to the intersection of the following two frequency ranges

$$[\omega_1, \omega_2] = [\omega_{1e} = \omega_\varepsilon, \omega_{2e} = \omega_b] \cap [\omega_{1m} = \omega_a, \omega_{2m} = \omega_\mu] \tag{2.85}$$

Assuming the existence of such intersection and admitting $\omega_\varepsilon < \omega_a < \omega_b < \omega_\mu$, we will get simply $\omega_1 = \omega_a$ and $\omega_2 = \omega_b$. The media will be DNG in the interval $[\omega_1 = \omega_a, \omega_2 = \omega_b]$.

Chapter 3

Wave Propagation in DNG Media

In this chapter, the propagation of a complex interface, that contains DNG and DPS media is studied. The modal characterization of this planar structures is analyzed as well as several numerical simulations and are results explained.

3.1 Propagation on a Planar DNG-DPS Interface

An unlimited isotropic DNG media has different electromagnetic properties than those found on DPS media. The propagation of electromagnetic waves in a complex structure, containing the interface between a DPS and a DNG media, allows the reflection and the refraction of backward waves. The propagation of electromagnetic waves on a planar interface between a DPS medium and a DNG semi-infinitive medium, here represented in Figure 3.1, will be analyzed in this section. Including the Modal Equations and Surface Mode Propagation. For the **Transverse Electric (TE)** waves, we have only E_y, H_x and H_z components,

while in the **Transverse Magnetic (TM)** only H_y, E_x and E_z propagate.

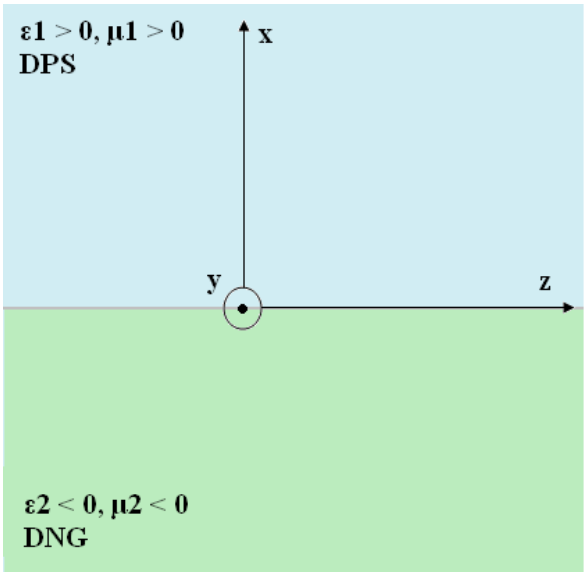

Figure 3.1: Planar interface between a DPS medium and a DNG medium.

3.1.1 Model Equations

We will consider the propagation direction along the z-axis, the transverse direction the x-axis and the transverse infinite direction by the y-axis, where there is no variation of both the electric and magnetic fields, $\frac{\partial}{\partial y} = 0$. The Maxwell equations are given by:

$$\nabla \times \mathbf{H} = \mathbf{J} + \frac{\partial \mathbf{D}}{\partial t} \tag{3.1}$$

$$\nabla \times \mathbf{E} = -\frac{\partial \mathbf{B}}{\partial t} \tag{3.2}$$

$$\nabla \cdot \mathbf{D} = \rho \tag{3.3}$$

$$\nabla \cdot \mathbf{E} = 0 \tag{3.4}$$

Since the results in the frequency domain are more clarifying than those in the time domain, we use the Fourier transform pair (3.5) and (3.6), to transform both $\mathbf{E}$ and $\mathbf{H}$ in to the frequency domain:

$$\mathbf{T}_\omega(\mathbf{r},\omega) = \int_{-\infty}^{+\infty} \mathbf{t}_\omega(\mathbf{r},t)\exp[i\omega t]dt \tag{3.5}$$

And the inverse equation:

$$\mathbf{t}_\omega(\mathbf{r},t) = \frac{1}{2\pi}\int_{-\infty}^{+\infty} \mathbf{T}_\omega(\mathbf{r},\omega)\exp[-i\omega t]dt \tag{3.6}$$

So, in the frequency domain, the Maxwell equations can be re-written to:

$$\nabla \times \mathbf{H} = \mathbf{J} + i\omega\mathbf{D} \tag{3.7}$$

$$\nabla \times \mathbf{E} = -i\omega\mathbf{B} \tag{3.8}$$

$$\nabla \cdot \mathbf{D} = \rho \tag{3.9}$$

$$\nabla \cdot \mathbf{E} = 0 \tag{3.10}$$

Along the z-axis the surface is homogeneous, we get the following solutions to the wave equation:

$$\mathbf{E}(x,t) = \mathbf{E}_m(x)\exp[i(\beta\, z - \omega\, t)] \tag{3.11}$$

$$\mathbf{H}(x,t) = \mathbf{H}_m(x)\exp[i(\beta\, z - \omega\, t] \tag{3.12}$$

And, for the time harmonic form of the fields:

$$\mathbf{E}(x,t) = \mathbf{E}_m(x)\exp[i\,\beta\, z] \tag{3.13}$$

$$\mathbf{H}(x,t) = \mathbf{H}_m(x)\exp[i\,\beta\, z] \tag{3.14}$$

Using the general field solutions, (3.13) and (3.14), in the **Homogeneous Wave Equation**, we get the **TE mode**, which is given by the following equations:

$$\nabla^2\mathbf{E} + \omega^2\varepsilon\,\mu\,\mathbf{E} = 0 \tag{3.15}$$

$$\frac{\partial^2}{\partial x^2}\mathbf{E} + \frac{\partial^2}{\partial z^2}\mathbf{E} + (k_0^2\, n_i^2)\mathbf{E} = 0 \tag{3.16}$$

$$\frac{\partial^2}{\partial x^2}\mathbf{E} + (k_0^2\, n_i^2 + \beta^2)\mathbf{E} = 0 \tag{3.17}$$

With n_i being the refraction index of the medium i, given by $n_i = \sqrt{\varepsilon_i\,\mu_i}$, and β is the propagation constant. Since $(k_0^2\, n_i^2 + \beta^2)$ is constant in x we are dealing with constant coefficient differential equation that could have the following solution:

$$\mathbf{E}_y(x) = E_0\exp[i\,h_i\,x] + E_0\exp[-i\,h_i\,x] \tag{3.18}$$

Where h_i is the transverse wave number of the medium i, given by $h_i^2 = k_0^2 n_i^2 - \beta^2$.

To maintain wave guiding on the interface, the fields must be evanescent and decay with distance away from the separation surface. Because of this requirement, the propagation constant is in the range of $k_0\, n < \beta$, the propagation constant h_i is complex in both the regions and it is given by:

$$h_i = \pm i\, \alpha_i \tag{3.19}$$

Where α_i is the attenuation constant given by:

$$\alpha_i^2 = \beta^2 + k_0^2\, n_i^2 \tag{3.20}$$

The sign of h_i is chosen to represent the field decaying with the distance from the interface DPS and DNG. Assuming the interface on $x = 0$, the field's are given by:

$$\mathbf{E}_y(x) = \begin{cases} E_0 \exp[-\alpha_1 x] & ,\ x > 0 \\ \\ E_0 \exp[\alpha_2 x] & ,\ x < 0 \end{cases} \tag{3.21}$$

Where α_1 and α_2 are both > 0. To calculate the magnetic field, we use the Faraday's Law from the Maxwell Equations:

$$\nabla \times \mathbf{E} = i\omega\mu\mathbf{H} \tag{3.22}$$

$$\mathbf{H} = \frac{1}{i\omega\mu} \nabla \times \mathbf{E} \tag{3.23}$$

In our case, the **TE propagation mode**, we can re-write equation (3.23):

$$\mathbf{H}_z = \frac{1}{i\omega\mu}\frac{\partial E_y}{\partial x}\hat{z} \tag{3.24}$$

From (3.23) we obtain the expressions for the magnetic field in both regions:

$$\mathbf{H}_z(x) = \begin{cases} \frac{i\,E_0\alpha_1}{\omega\mu_1}\exp[-\alpha_1 x] & , x > 0 \\ \\ \frac{-i\,E_0\alpha_2}{\omega\mu_2}\exp[\alpha_2 x] & , x < 0 \end{cases} \tag{3.25}$$

For the boundary conditions, at $x = 0$, and to guarantee the continuity of the magnetic field at the interface, we need to assure $H_z(0)^- = H_z(0)^+$. To do so, we have the expression:

$$\frac{i\,E_0\alpha_1}{\omega\mu_1}\exp[-\alpha_1 0] = \frac{-i\,E_0\alpha_2}{\omega\mu_2}\exp[\alpha_1 0] \tag{3.26}$$

$$\frac{\alpha_1}{\mu_1} = \frac{-\alpha_2}{\mu_2} \tag{3.27}$$

And so,

$$\alpha_2\mu_1 + \alpha_1\mu_2 = 0 \tag{3.28}$$

With (3.27), we obtained the modal equation for the **TE mode** given by (3.28).

To obtain the modal equation for the TM mode, we can apply similar computation to the wave equation and field expressions for the TM modes, using the following equation from the Maxwell Equations,

$$\nabla \times \mathbf{H} = -i\omega\varepsilon\mathbf{E} \tag{3.29}$$

$$\mathbf{E} = \frac{1}{-i\omega\varepsilon}\nabla \times \mathbf{H} \tag{3.30}$$

Re-writing equation (3.30),

$$\mathbf{E} = \frac{1}{-i\omega\varepsilon}\frac{\partial H_y}{\partial x}\hat{z} \tag{3.31}$$

Applying (3.31) on (3.21)we get for the boundary condition, where $E_y(0)^- = E_y(0)^+$, the following expression,

$$\frac{-E_0}{-i\omega\varepsilon_1}\alpha_1 \exp[-\alpha_1 0] = \frac{E_0}{-i\omega\varepsilon_2}\alpha_2 \exp[\alpha_2 0] \tag{3.32}$$

And we get,

$$\alpha_2\varepsilon_1 + \alpha_1\varepsilon_2 = 0 \tag{3.33}$$

With the modal equations (3.28)and (3.33), we can conclude if there is propagation along the interface between a DPS medium and a DNG medium. Since we have α_1, $\alpha_2 > 0$ and μ_1,$\mu_2 > 0$, from (3.28), for the **TE mode**:

$$\alpha_1 = -\frac{\mu_1}{\mu_2}\alpha_2 > 0 \implies \mu_2 < 0 \tag{3.34}$$

And, from equation (3.33) we get for the **TM mode**:

$$\alpha_1 = -\frac{\varepsilon_1}{\varepsilon_2}\alpha_2 > 0 \implies \varepsilon_2 < 0 \tag{3.35}$$

From implications (3.34) and (3.35) we can conclude that there is propagation on an interface between a DPS medium and a DNG medium, with ε_2,$\mu_2 < 0$.

3.1.2 Surface Mode Propagation

To analyze the solutions of the modal equations we will use the **Lorentz Dispersive Model** (**LDM**). This model has permittivity and permeability dependent of the frequency. and the equations, from (2.81), are:

$$\varepsilon_{r,L}(\omega) = 1 + \frac{\omega_{pe}^2}{\omega_{0e}^2 - i\omega\Gamma - \omega^2} \tag{3.36}$$

$$\mu_{r,L}(\omega) = 1 + \frac{\omega_{pm}^2}{\omega_{0m}^2 - i\omega\Gamma - \omega^2} \tag{3.37}$$

This model is going to be used to describe the parameters, dependent of the frequency, on the DNG medium. Like we already done in the previous chapter, we remove the index e and the index m, and consider $\Gamma_L = \Gamma_e = \Gamma_m$. For the simulation we will use the following parameters, where $\varepsilon_{1,r}$ and $\mu_{1,r}$ are used to describe the DPS medium:

Parameter	**Value**
ω_{pe}	$2\pi \times 7 \times 10^9 rad.s^{-1}$
ω_{pm}	$2\pi \times 6 \times 10^9 rad.s^{-1}$
ω_{0e}	$2\pi \times 2.5 \times 10^9 rad.s^{-1}$
ω_{0m}	$2\pi \times 2.3 \times 10^9 rad.s^{-1}$
Γ_L	$0.05 \times \omega_{pe}$
$\varepsilon_{1,r}$	1
$\mu_{1,r}$	1

Table 3.1: Parameters used in the Lorentz Dispersive Model, on the DPS-DNG interface

3.1.2.1 Lossless Lorentz Dispersive Model

For a first approach lets simulate a lossless model (when $\Gamma_L = 0$), analyzing the variation of the parameters $\varepsilon_{r,L}(\omega)$ and $\mu_{r,L}(\omega)$. The results are in Figure3.2.

From Figure 2.1:

We identify the following three regions:

- **DNG** region when $\varepsilon < 0$ and $\mu < 0$;
- **ENG** region when $\varepsilon < 0$ and $\mu > 0$;
- and **DPS** when $\varepsilon > 0$ and $\mu > 0$.

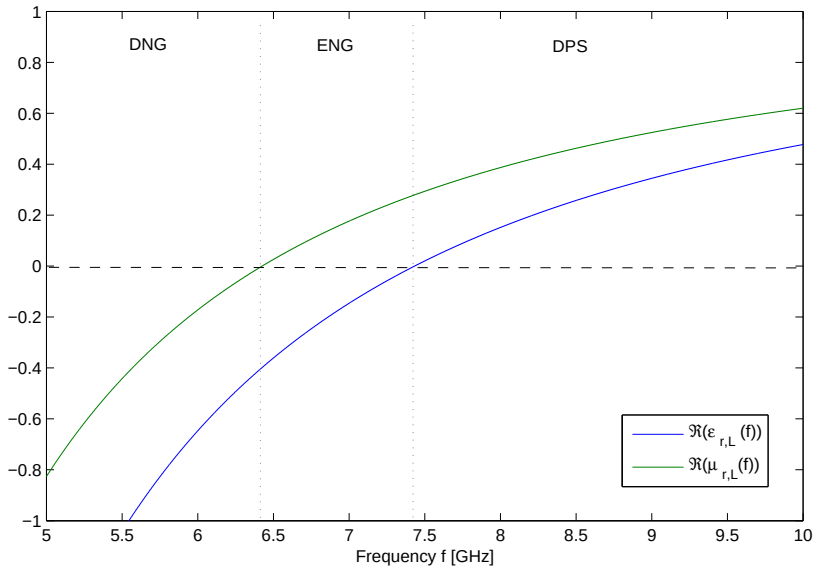

Figure 3.2: Lossless Lorentz Dispersive model for $\varepsilon_{r,L}$ and $\mu_{r,L}$

To observe the above three regions, we analyze the relative refraction index, given by (3.38), using the lossless LDM on the DPS-DNG interface.

$$n_r = \frac{n}{\sqrt{\varepsilon_0 \mu_0}} \tag{3.38}$$

By simulation, seen in Figure 3.3, we can denote that n varies with the frequency. This effect is known as **dispersion** and only occurs when a media is present, in vacuum all the frequencies travel at the same speed, c, the speed of light. We also can identify the three already mentioned regions: the DNG region with negative refraction index and the DPS with positive refraction. The

ENG region, since the permittivity is negative and the permeability is positive, has purely imaginary refraction index.

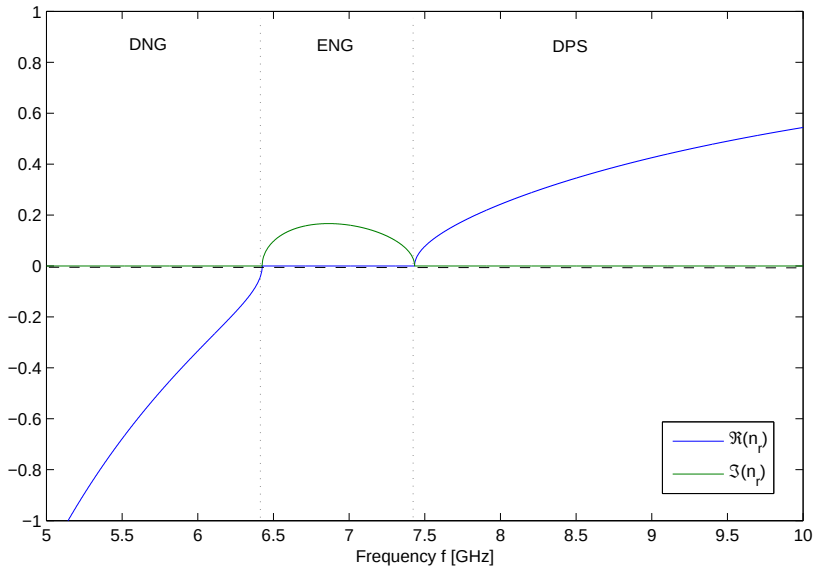

Figure 3.3: Relative refraction index for DPS and DNG medium using the lossless LDM

To get the **dispersion relation**, which expresses the relation between the propagation constant β and the frequency, we use, for the **TE** mode, the equations (3.20) and (3.28):

$$\alpha_2 = \frac{\mu_2}{\mu_1}\,\alpha_1 \tag{3.39}$$

Applying (3.20) to both α_1 and α_2,

$$\sqrt{\beta(\omega)^2 + k_0^2\, n_2^2} = (-\frac{\mu_2(\omega)}{\mu_1})\,\sqrt{\beta(\omega)^2 + k_0^2\, n_1^2} \tag{3.40}$$

$$\beta(\omega)^2 + k_0^2\, n_2^2 = (\frac{\mu_2(\omega)}{\mu_1})^2\,\beta(\omega)^2 + (\frac{\mu_2(\omega)}{\mu_1})^2(k_0^2\, n_1^2) \tag{3.41}$$

$$\beta(\omega)^2(1-(\frac{\mu_2(\omega)}{\mu_1})^2) = (\frac{\mu_2(\omega)}{\mu_1})^2(k_0^2 n_1^2) - (k_0^2 n_2^2) \tag{3.42}$$

$$\beta(\omega)^2 = \frac{(\frac{\mu_2(\omega)}{\mu_1})^2 n_1^2 - n_2^2}{1-(\frac{\mu_2(\omega)}{\mu_1})^2}\, k_0^2 \tag{3.43}$$

$$\beta(\omega) = \pm\sqrt{\frac{(\frac{\mu_2(\omega)}{\mu_1})^2 n_1^2 - n_2^2}{1-(\frac{\mu_{2(\omega)}}{\mu_1})^2}}\, k_0 \tag{3.44}$$

Since,

$$n_1 = \sqrt{\mu_1 \varepsilon_1} \tag{3.45}$$

And

$$n_2 = \sqrt{\mu(\omega)\, \varepsilon_2(\omega)} \tag{3.46}$$

We get,

$$\beta(\omega) = \sqrt{\frac{(\frac{\mu_2(\omega)}{\mu_1})^2 \mu_1 \varepsilon_1 - \mu_2(\omega)\varepsilon_2(\omega)}{1-(\frac{\mu_2(\omega)}{\mu_1})^2}}\, k_0 \tag{3.47}$$

Which is the **dispersion relation** for the **TE mode**. For the **TM mode**, we use the equations (3.20) and (3.33) resulting in:

$$\beta(\omega) = \sqrt{\frac{(\frac{\varepsilon_2(\omega)}{\varepsilon_1})^2 \mu_1 \varepsilon_1 - \mu_2(\omega)\varepsilon_2(\omega)}{1-(\frac{\varepsilon_2(\omega)}{\varepsilon_1})^2}}\, k_0 \tag{3.48}$$

Applying the Lorentz Dispersive Model, given by 3.36 and (3.37), on both (3.47) and (3.48) we can obtain the graphical simulation for the dispersion relation. The TM mode is represented in Figure 3.4 and the TE mode in Figure 3.5.

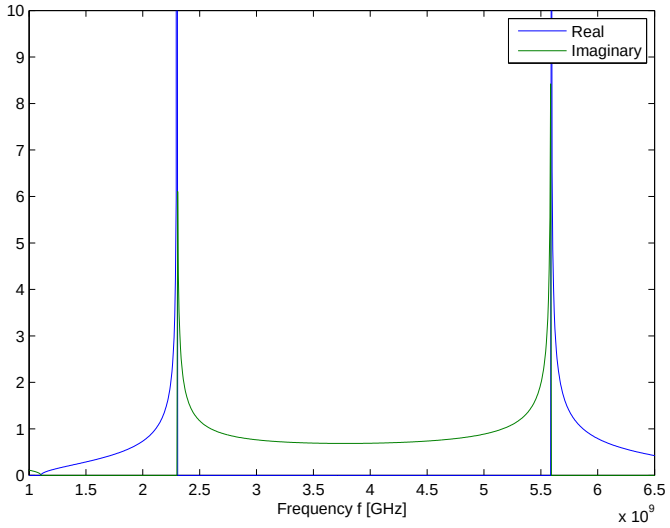

Figure 3.4: Dispersion relation β for the TM mode

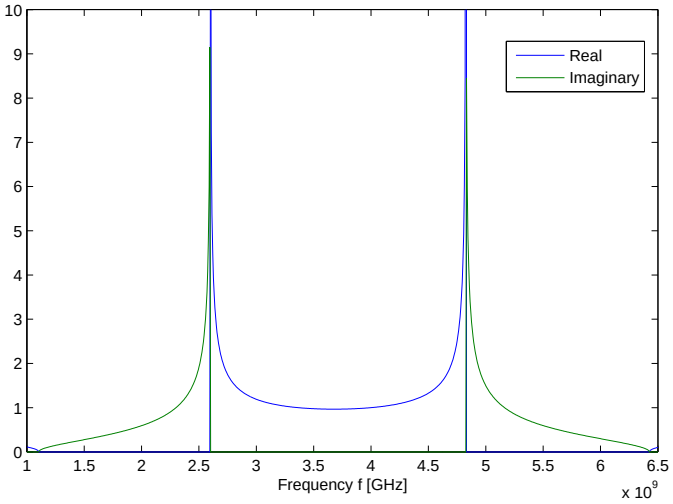

Figure 3.5: Dispersion relation β for the TE mode

The simulations for the dispersion relation, for TM and TE modes, is just a theoretic exercise since there is no physical meaning for them. As we know,

dispersion only occurs in a lossy model. For this reason, both modes have asymptotes.

Now, we can get the frequency dependent attenuation constants α_1 and α_2 using the lossless LDM for a DPS-DNG interface. For the TM mode, from (3.20), (3.33) and (3.47),

$$\alpha_i^2 = \delta\, k_0^2 + k_0^2\, n_i^2 \tag{3.49}$$

$$\alpha_i = \sqrt{\delta + n_i^2}k_0 \tag{3.50}$$

Considering for TM mode :

$$\delta = \frac{(\frac{\varepsilon_2(\omega)}{\varepsilon_1})^2\mu_1\varepsilon_1 - \mu_2(\omega)\varepsilon_2(\omega)}{1 - (\frac{\varepsilon_2(\omega)}{\varepsilon_1})^2} \tag{3.51}$$

The attenuation constant α_1 is given by:

$$\alpha_1 = \sqrt{\delta + n_1^2}k_0 \tag{3.52}$$

$$\alpha_1 = \sqrt{\frac{(\frac{\varepsilon_2(\omega)}{\varepsilon_1})^2\mu_1\varepsilon_1 - \mu_2(\omega)\varepsilon_2(\omega)}{1 - (\frac{\varepsilon_2(\omega)}{\varepsilon_1})^2} + \varepsilon_1\mu_1}k_0 \tag{3.53}$$

$$\alpha_1 = \sqrt{\frac{(\frac{\varepsilon_2(\omega)}{\varepsilon_1})^2\mu_1\varepsilon_1 - \mu_2(\omega)\varepsilon_2(\omega) + \varepsilon_1\mu_1 - (\frac{\varepsilon_2(\omega)}{\varepsilon_1})^2\varepsilon_1\mu_1}{1 - (\frac{\varepsilon_2(\omega)}{\varepsilon_1})^2}}k_0 \tag{3.54}$$

$$\alpha_1 = \sqrt{\frac{\varepsilon_1\mu_1 - \mu_2(\omega)\varepsilon_2(\omega)}{1 - (\frac{\varepsilon_2(\omega)}{\varepsilon_1})^2}}k_0 \tag{3.55}$$

For α_2 we get,

$$\alpha_2 = \sqrt{\frac{(\frac{\varepsilon_2(\omega)}{\varepsilon_1})^2\mu_1\varepsilon_1 - \mu_2(\omega)\varepsilon_2(\omega)}{1-(\frac{\varepsilon_2(\omega)}{\varepsilon_1})^2} + \varepsilon_2(\omega)\,\mu_2(\omega)k_0} \tag{3.56}$$

$$\alpha_2 = \sqrt{\frac{(\frac{\varepsilon_2(\omega)}{\varepsilon_1})^2\mu_1\varepsilon_1 - \mu_2(\omega)\varepsilon_2(\omega) + \mu_2(\omega)\varepsilon_2(\omega) - (\frac{\varepsilon_2(\omega)}{\varepsilon_1})^2\mu_2(\omega)\varepsilon_2(\omega)}{1-(\frac{\varepsilon_2(\omega)}{\varepsilon_1})^2}}k_0 \tag{3.57}$$

$$\alpha_2 = \sqrt{\frac{(\frac{\varepsilon_2(\omega)}{\varepsilon_1})^2(\mu_1\varepsilon_1 - \mu_2(\omega)\varepsilon_2(\omega))}{1-(\frac{\varepsilon_2(\omega)}{\varepsilon_1})^2}}k_0 \tag{3.58}$$

And similarly, for the TE mode using (3.50) and a δ given by: :

$$\delta = \frac{(\frac{\mu_2(\omega)}{\mu_1})^2\mu_1\varepsilon_1 - \mu_2(\omega)\varepsilon_2(\omega)}{1-(\frac{\mu_2(\omega)}{\mu_1})^2} \tag{3.59}$$

We have,

$$\alpha_1 = \sqrt{\frac{\varepsilon_1\mu_1 - \mu_2(\omega)\varepsilon_2(\omega)}{1-(\frac{\mu_2(\omega)}{\mu_1})^2}}k_0 \tag{3.60}$$

And,

$$\alpha_2 = \sqrt{\frac{(\frac{\mu_2(\omega)}{\mu_1})^2(\mu_1\varepsilon_1 - \mu_2(\omega)\varepsilon_2(\omega))}{1-(\frac{\mu_2(\omega)}{\mu_1})^2}}k_0 \tag{3.61}$$

The graphical representation of the above attenuation constants is represented in Figure 3.6 and Figure 3.7.

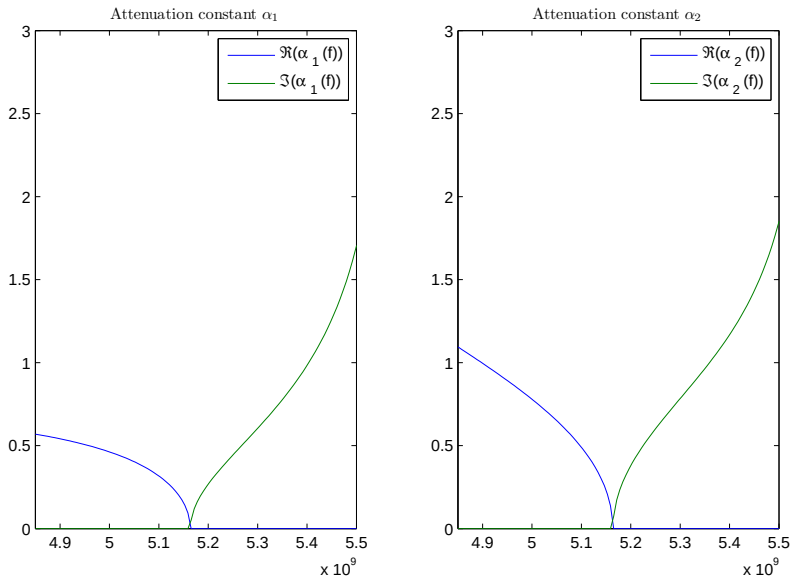

Figure 3.6: Attenuation constants α_1 and α_2 for the TM mode for the lossless LDM

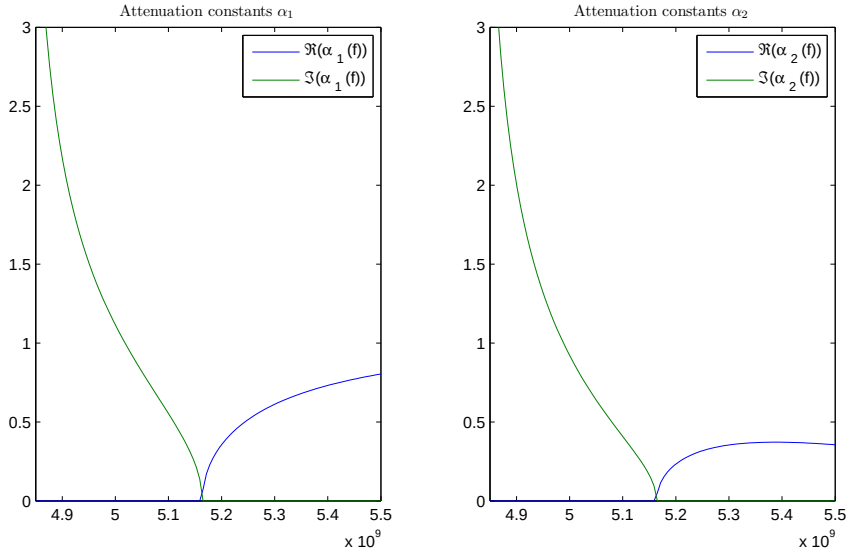

Figure 3.7: Attenuation constants α_1 and α_2 for the TE mode for the lossless LDM

3.1.2.2 Lossy Lorentz Dispersive Model

To a more realistic study, we will include losses on the complex structure using the LDM. Using (3.36) and (3.37), with $\Gamma_L = 0.05\,\omega_{pe}$, the permittivity and permeability on the DNG medium can be graphically by Figure 3.8.

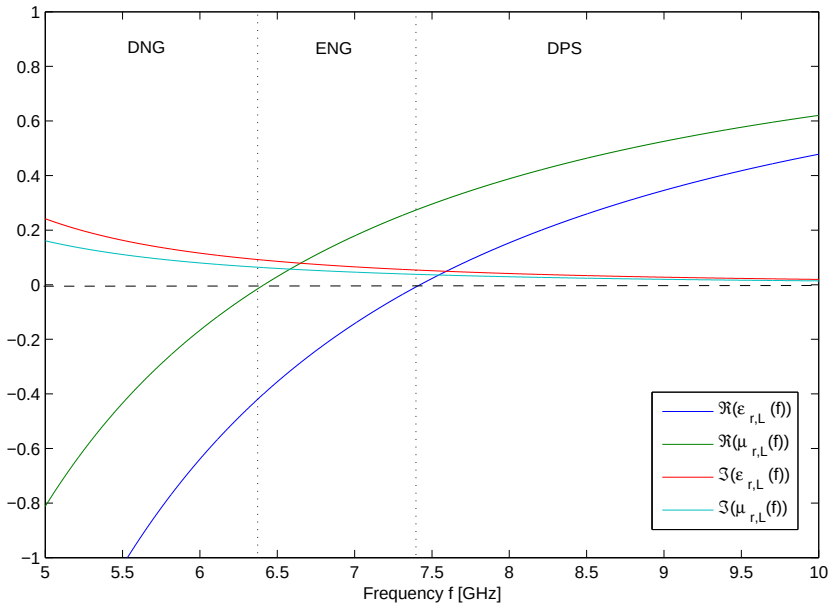

Figure 3.8: Lossy Lorentz Dispersive model for $\varepsilon_{r,L}$ and $\mu_{r,L}$

The three regions (DNG, ENG and DPS) occur at almost the same frequencies than in the lossless model due to the use of small value of Γ_L.The "negative" damping present on the LDM results in the positive imaginary parts.

Now for lossy relative refraction index, given by (3.38) we obtain the following graphical result:

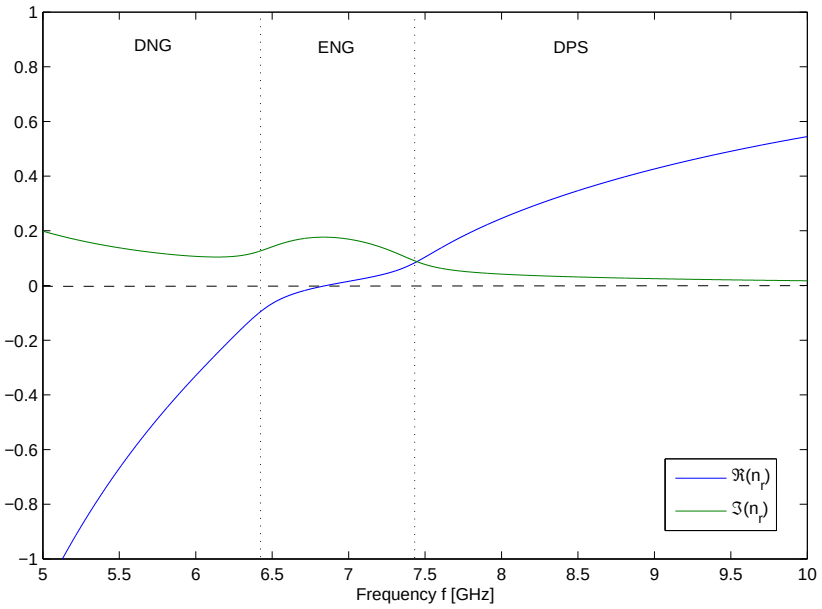

Figure 3.9: Relative refraction index for DPS and DNG medium using the lossy LDM

In Figure 3.9 we can observe the already mentioned three regions. Where the DNG region has a negative refraction index and the DPS region has positive refraction index. These were the expected results, but from the ENG region, since it has a negative real refraction index, we can conclude that a DNG medium is always a Negative Refraction Index (**NRI**) but a NRI medium does not mean a DNG medium if we consider losses and dispersion.

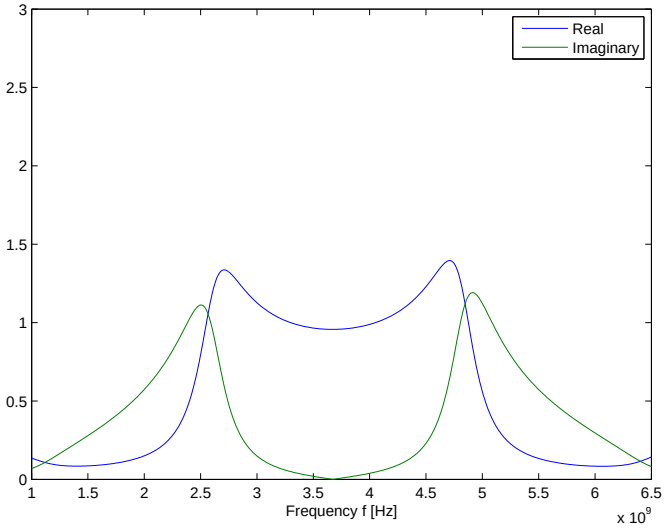

Figure 3.10: Lossy dispersion relation β for the TE modes

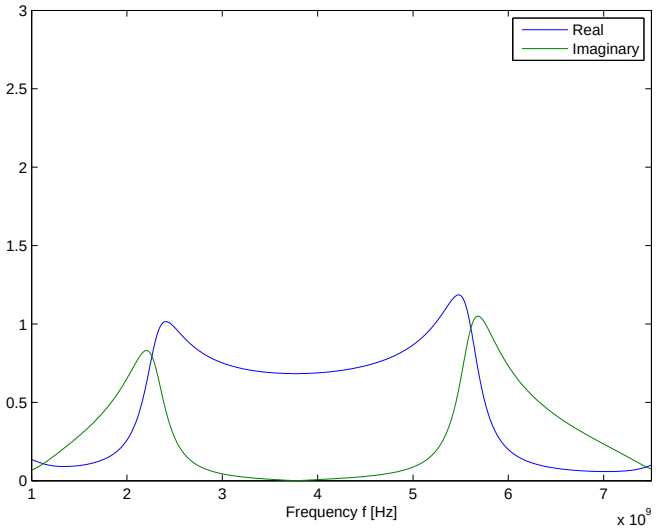

Figure 3.11: Lossy dispersion relation β for the TM modes

The graphical representation of the attenuation constants for the TE modes,

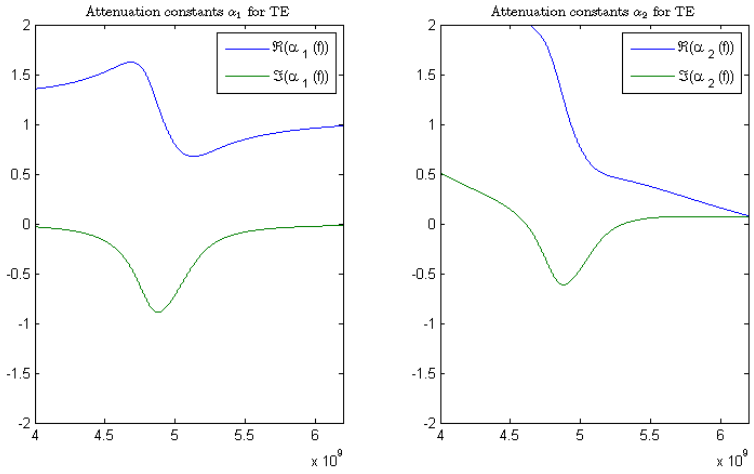

Figure 3.12: Attenuation constants α_1 and α_2 for the TE modes for the lossy LDM

And for the TM modes,

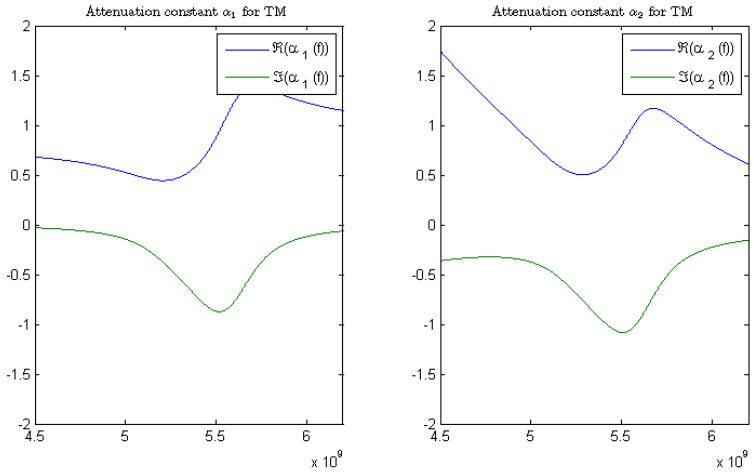

Figure 3.13: Attenuation constants α_1 and α_2 for the TM modes for the lossly LDM

We can also have a graphical representation of the electric field's variation

along the x-axis dimension. The variation of the field shows us that the field intensity increases as we approach $x = 0$, as we expected, because this is a representation of the field in the interface (which is at $x = 0$) and the attenuation as we get further from it.

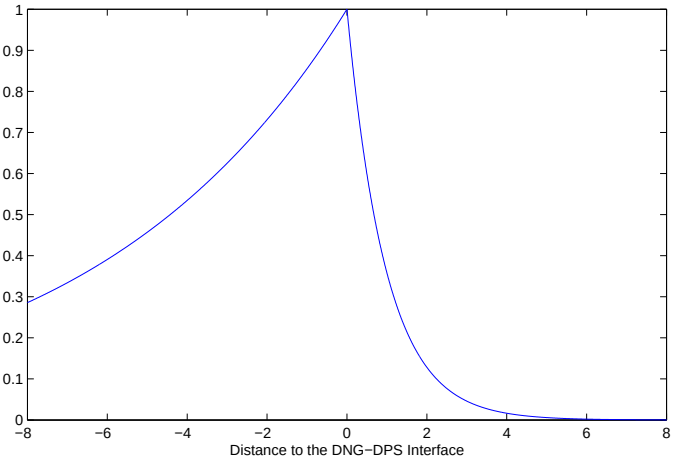

Figure 3.14: Variation of the normalized Electric Field for $f = 1.10\,GHz$

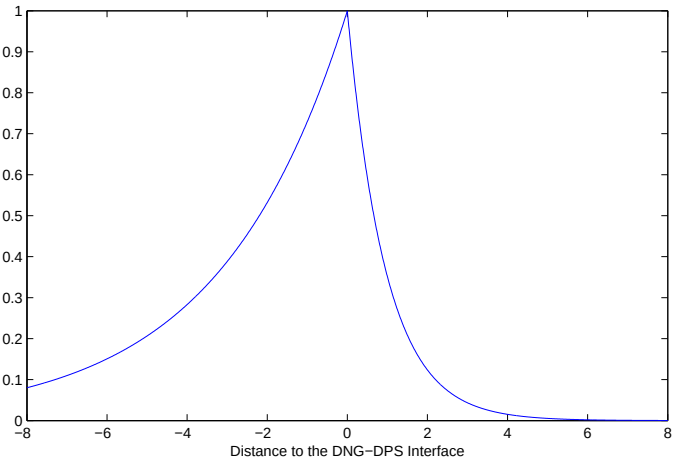

Figure 3.15: Variation of the normalized Electric Field for $f = 1.20\,GHz$

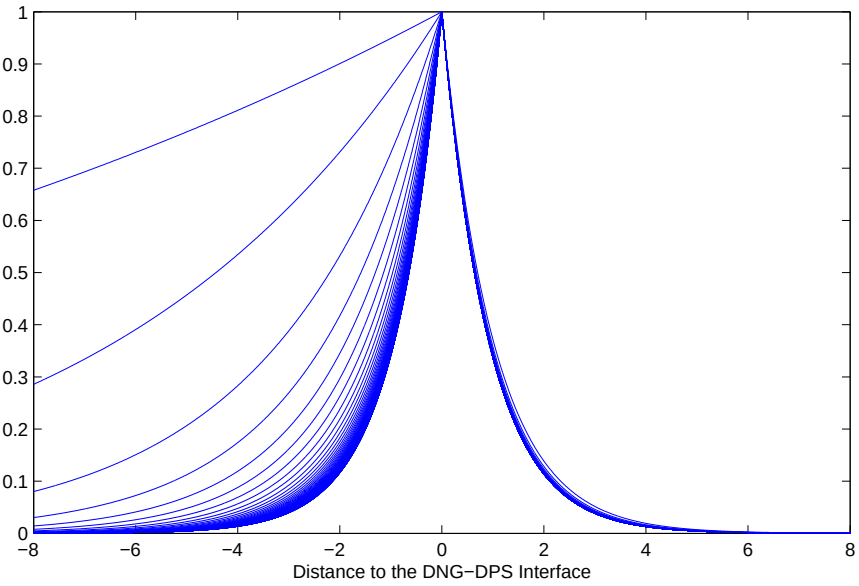

Figure 3.16: Variation of the normalized Electric Field for a frequency range of $f : [1, 10]GHz$ with $100\,MHz$ intervals.

Since we use the Lorentz Dispersive Model, both the permittivity ε and permeability μ, as seen on Figure 3.8, from certain value of the frequency f, tends asymptotically to a value, 1. This "stability" has direct influence on the electric field E_y of Figure 3.16 where, for higher values of f, E_y also tends tends asymptotically.

3.2 Existence of Solution Bands

The key issue for the practical implementation of a DNG metamaterial has to do with necessity to assure that the resonances of $\varepsilon(\omega)$ and $\mu(\omega)$ are close enough to each other. An acceptable model lossless model is studied in the present section.

Considering the interface between air and a metamaterial at $x = 0$, with the metamaterial medium characterized by the following constitutive relations,

$$\mathbf{D} = \varepsilon_0 \varepsilon(\omega)\mathbf{E} \tag{3.62}$$

$$\mathbf{B} = \mu_0 \mu(\omega)\mathbf{H} \tag{3.63}$$

With,

$$\begin{cases} \varepsilon(\omega) = 1 - \frac{\omega_p^2}{\omega^2} \\ \\ \mu(\omega) = 1 - F\frac{\omega^2}{\omega^2 - \omega_0^2} \end{cases} \tag{3.64}$$

As seen in Figure 3.1, the air, defined as 1, occupies the region $x > 0$ while the metamaterial medium is defined as 2 and occupies the region $x < 0$. Considering the propagation modes TE and TM in the form $exp[i\,(\beta\, z - \omega\, t)]$ along this interface.

Assuming,

$$X = \frac{\omega_p^2}{\omega^2} \tag{3.65}$$

$$a = \frac{\omega_0^2}{\omega_p^2} \tag{3.66}$$

We get, after applying (3.65) and (3.66) on (3.64),

$$\begin{cases} \varepsilon(X) = 1 - X \\ \\ \mu(X) = 1 - F\frac{1}{1-a\,X} \end{cases} \tag{3.67}$$

Where F , $0 < F < 1$, is the filling factor for the model and a the square of the relation between the magnetic resonance frequency, ω_0, and the plasma frequency, ω_p .

There are some points of interest, like the resonance of $\mu(X)$ at $X = 1/a$ and the root at $X = (1-F)/a$. $\mu(X)$ has the same root as $\varepsilon(X)$ when $F/(1-a) = 1$. Therefore, we can now characterize this interface in different combinations of media regions, depending of the values of F or a.

Fixing the value of $a = 0.36$, to study the interface by regions of medium classification, we have, according to Figure 2.1, the following

$0 < X < 1$	DPS
$1 < X < \frac{1-F}{a}$	ENG
$\frac{1-F}{a} < X < \frac{1}{a}$	DNG
$X > \frac{1}{a}$	ENG

Table 3.2: Classification of the metamaterial's regions for various $0 < F < 0.64$

$0 < X < 1$	DPS
$1 < X < \frac{1}{a}$	DNG
$X > 1$	ENG

Table 3.3: Classification of the metamaterial's regions for various $F = 0.64$

$0 < X < \frac{1-F}{a}$	DPS
$\frac{1-F}{a} < X < 1$	MNG
$1 < X < \frac{1}{a}$	DNG
$X > \frac{1}{a}$	ENG

Table 3.4: Classification of the metamaterial's regions for various $0.64 < F < 1.0$

After simulating $\varepsilon(X)$ and $\mu(X)$ for some values of F with $\omega \geq 0$ (and therefore $X \geq 0$) and $a = 0.36$, we obtained the following,

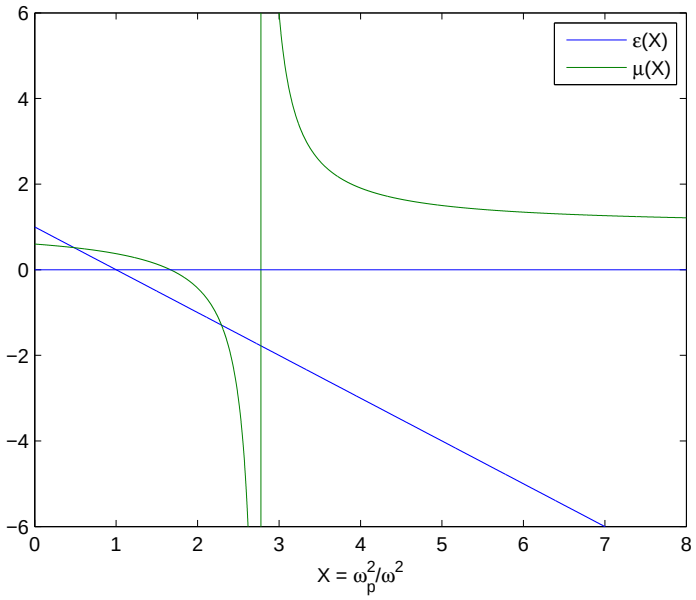

Figure 3.17: $\varepsilon - vs - \mu$ representation for $F = 0.40$

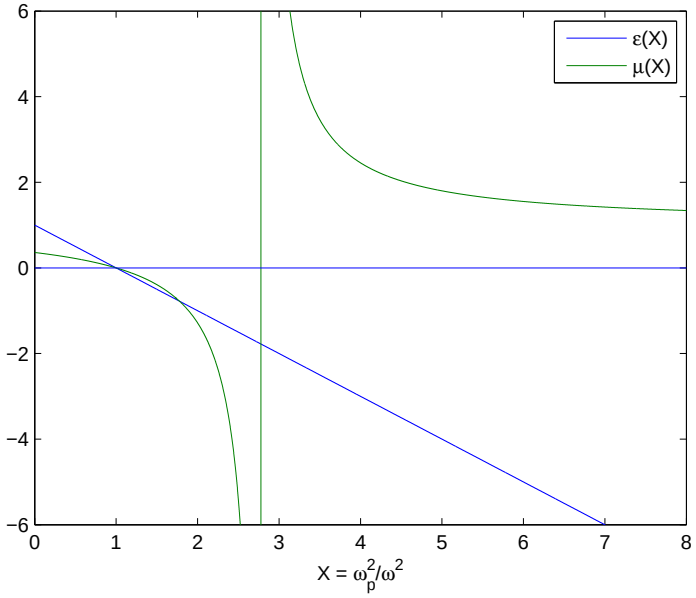

Figure 3.18: $\varepsilon - vs - \mu$ representation for $F = 0.64$

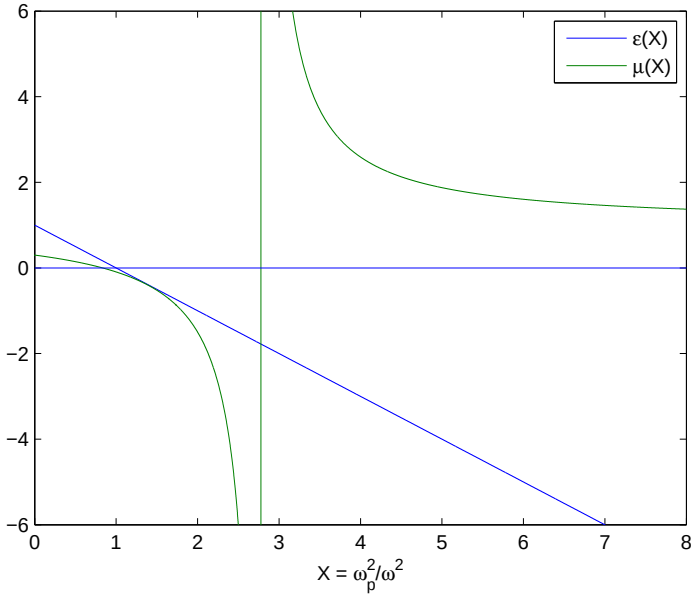

Figure 3.19: $\varepsilon - vs - \mu$ representation for $F = 0.70$

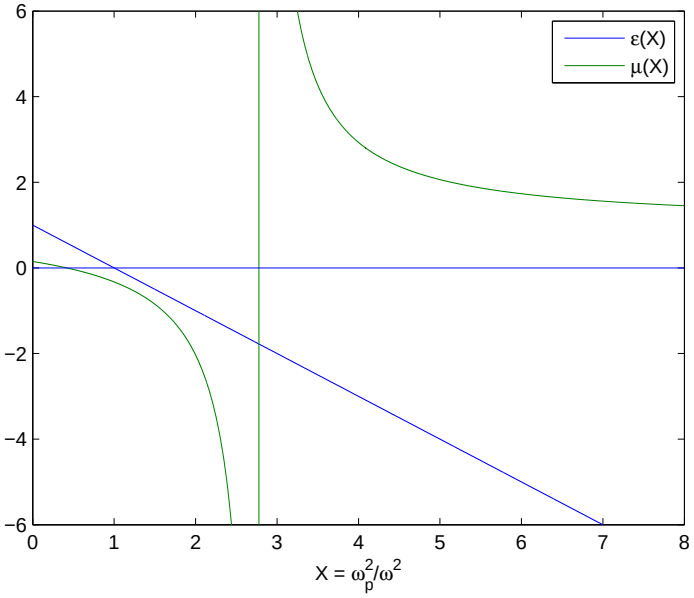

Figure 3.20: $\varepsilon - vs - \mu$ representation for $F = 0.85$

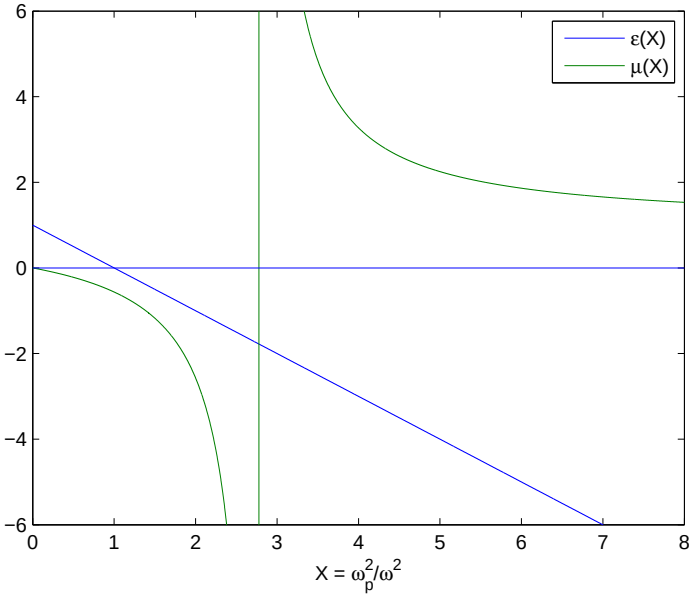

Figure 3.21: $\varepsilon - vs - \mu$ representation for $F = 1.0$

If, instead of having a fixed value of a, we consider the fixed value of $F = 0.56$, we have the following medium classification

$0 < X < 1$	DPS
$1 < X < \frac{1-F}{a}$	ENG
$\frac{1-F}{a} < X < \frac{1}{a}$	DNG
$X > \frac{1}{a}$	ENG

Table 3.5: Classification of the metamaterial's regions for $0 < a < 0.44$

$0 < X < 1$	DPS
$1 < X < \frac{1}{a}$	DNG
$X > 1$	ENG

Table 3.6: Classification of the metamaterial's regions for $a = 0.44$

$0 < X < \frac{1-F}{a}$	DPS
$\frac{1-F}{a} < X < 1$	MNG
$1 < X < \frac{1}{a}$	DNG
$X > \frac{1}{a}$	ENG

Table 3.7: Classification of the metamaterial's regions for various $a > 0.44$

After simulating $\varepsilon(X)$ and $\mu(X)$ for some values of a with $\omega \geq 0$ and $F = 0.56$, we obtain the following,

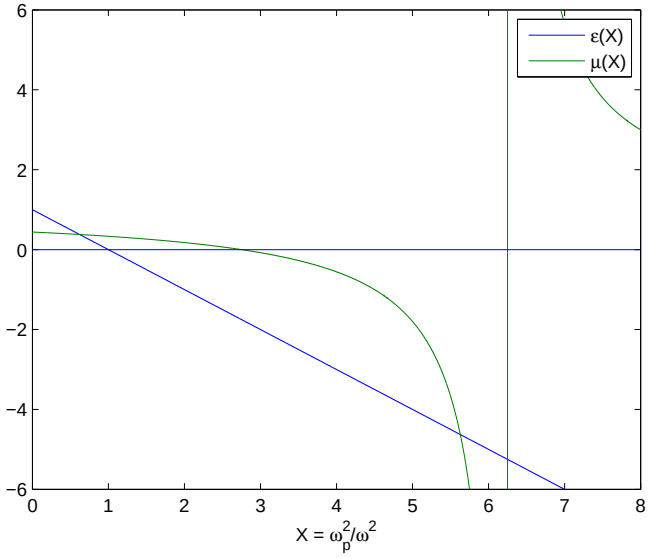

Figure 3.22: $\varepsilon - vs - \mu$ representation for $a = 0.16$

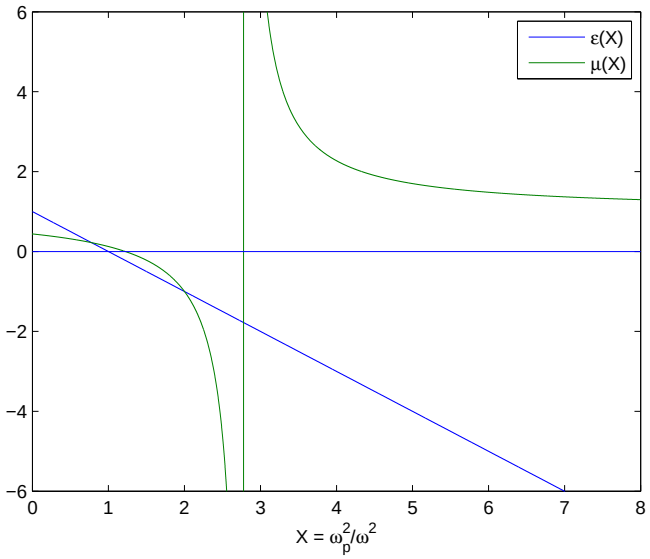

Figure 3.23: $\varepsilon - vs - \mu$ representation for $a = 0.36$

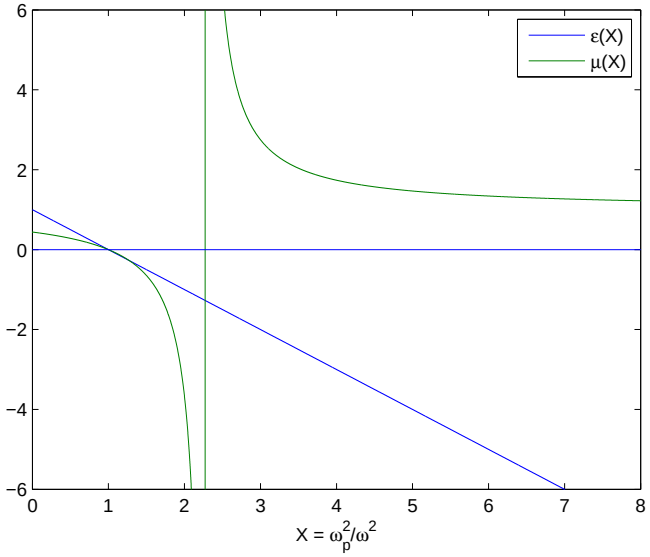

Figure 3.24: $\varepsilon - vs - \mu$ representation for $F = 0.44$

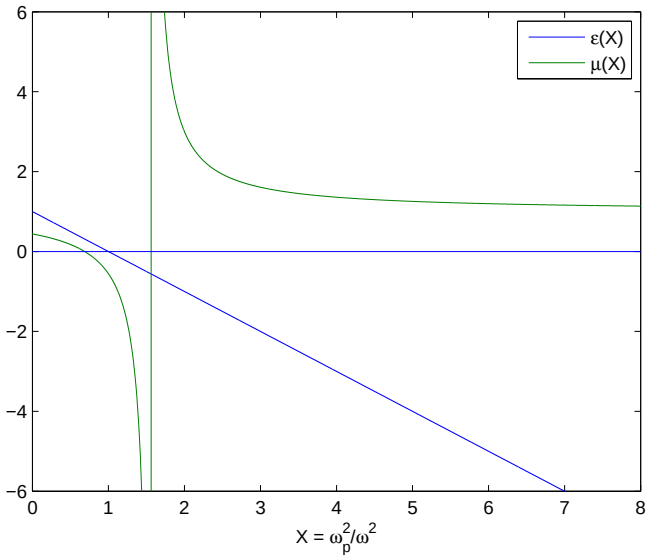

Figure 3.25: $\varepsilon - vs - \mu$ representation for $F = 0.64$

3.3 Modal Refraction Index $\bar{n}$

In this section, we will study the relation between $\bar{n}$, the modal refraction index, and ε and μ, where $\overline{n}$ is given by,

$$\overline{n} = \frac{\beta}{k_0} \tag{3.68}$$

The sourceless Maxwell equations can be, in this case, reduced to,

$$\begin{cases} -i\beta E_y = i\omega\mu_0\mu(x)\, H_x \\ i\beta E_x - \frac{\partial E_Z}{\partial x} = i\omega\mu_0\mu(x)\, H_y \\ \frac{\partial E_y}{\partial x} = i\omega\mu_0\mu(x)\, H_z \end{cases} \tag{3.69}$$

$$\begin{cases} -i\beta H_y = -i\omega\varepsilon_0\mu(x)\, E_x \\ i\beta H_x - \frac{\partial H_Z}{\partial x} = -i\omega\varepsilon_0\varepsilon(x)\, E_y \\ \frac{\partial H_y}{\partial x} = -i\omega\varepsilon_0\varepsilon(x)\, H_z \end{cases} \tag{3.70}$$

For TE modes, the only non-zero components are E_y, H_x and H_z. For TM modes the only non-zero components are H_y, E_x and E_z. Therefore, for the TE mode we have,

$$\begin{cases} H_x = -\frac{\beta}{\omega\mu_0\mu(x)} E_y \\ H_z = -i\frac{1}{\omega\mu_0\mu(x)} \frac{\partial E_y}{\partial x} \end{cases} \tag{3.71}$$

And, similarly, for the TM mode,

$$\begin{cases} E_x = \frac{\beta}{\omega\varepsilon_0\varepsilon(x)} H_y \\ \\ E_z = i\frac{1}{\omega\varepsilon_0\varepsilon(x)} \frac{\partial E_y}{\partial x} \end{cases} \tag{3.72}$$

For both cases, the differential equation for the "support" component has the form,

$$\left\{ \frac{\partial^2}{\partial x^2} + \left[\varepsilon(x)\mu(x)k_0^2 + \beta\right] \right\} \begin{Bmatrix} E_y \\ H_y \end{Bmatrix} = 0 \tag{3.73}$$

With,

$$k_0^2 = \omega^2\varepsilon_0\mu_0 = \left(\frac{\omega}{c}\right)^2 \tag{3.74}$$

This way, we got

$$\left[\frac{\partial^2}{\partial x^2} - \alpha^2(x) \right] \begin{Bmatrix} E_y \\ H_y \end{Bmatrix} = 0 \tag{3.75}$$

$$\alpha^2(x) = \beta^2 - \varepsilon(x)\mu(x)k_0^2 \tag{3.76}$$

Where,

$$\begin{cases} \alpha_1^2 = \beta^2 - k_0^2 & , x > 0 \\ \\ \alpha_2^2 = \beta^2 - \varepsilon(x)\mu(x)k_0^2 & , x < 0 \end{cases} \tag{3.77}$$

So, for the **TE modes**,

$$E_y(x) = \begin{cases} \exp(-\alpha_1 x) & , x > 0 \\ \\ \exp(\alpha_2 x) & , x > 0 \end{cases} \tag{3.78}$$

And, for the **TM modes**,

$$H_y(x) = \begin{cases} \exp(-\alpha_1 x) & , x > 0 \\ \\ \exp(\alpha_2 x) & , x > 0 \end{cases} \tag{3.79}$$

Although the continuity is assured for the support component, for TE modes the continuity is yet to be imposed to H_z at $x = 0$:

$$\frac{1}{\mu(\omega)} \frac{\partial E_y}{\partial x}|_{x=0^-} = \frac{\partial E_y}{\partial x}|_{x=0^+} \ \rightarrow \mu(\omega)\alpha_1 + \alpha_2 = 0 \tag{3.80}$$

In the TM modes, we need to impose the continuity of E_z at $x = 0$:

$$\frac{1}{\varepsilon(\omega)} \frac{\partial H_y}{\partial x}|_{x=0^-} = \frac{\partial H_y}{\partial x}|_{x=0^+} \ \rightarrow \varepsilon(\omega)\alpha_1 + \alpha_2 = 0 \tag{3.81}$$

This way, the TE modes only occurs in regions where $\mu(X) < 0$ and the TM modes only occur in regions where $\varepsilon(X) > 0$. When the metamaterial is DNG, both TE and TM modes can propagate.

So, for the TE modes, we got

$$\mu^2(\omega)\alpha_1^2 = \alpha_2^2 \ \rightarrow \ \mu^2(\omega)(\beta^2 - k_0^2) = \beta^2 - \varepsilon(\omega)\mu(\omega)k_0^2 \tag{3.82}$$

$$\beta^2 = \frac{\varepsilon(\omega)\mu(\omega) - \mu^2(\omega)}{1 - \mu^2(\omega)} k_0^2 \tag{3.83}$$

$$\mu(\omega) = -\,|\mu(\omega)| \tag{3.84}$$

$$\boxed{\text{TE} \longmapsto \overline{n}^2 = \left(\frac{\beta}{k_0}\right)^2 = \frac{\mu(\omega)}{1+\mu(\omega)}\frac{\varepsilon(\omega)-\mu(\omega)}{1-\mu(\omega)} = |\mu(\omega)|\,\frac{|\mu(\omega)|+\varepsilon(\omega)}{\mu^2(\omega)-1}} \tag{3.85}$$

for the TM modes, we got

$$\varepsilon^2(\omega)\alpha_1^2 = \alpha_2^2 \;\rightarrow\; \varepsilon^2(\omega)(\beta^2 - k_0^2) = \beta^2 - \varepsilon(\omega)\mu(\omega)k_0^2 \tag{3.86}$$

$$\beta^2 = \frac{\varepsilon(\omega)\mu(\omega) - \varepsilon^2(\omega)}{1-\varepsilon^2(\omega)}k_0^2 \tag{3.87}$$

$$\varepsilon(\omega) = -\,|\varepsilon(\omega)| \tag{3.88}$$

$$\boxed{\text{TM} \longmapsto \overline{n}^2 = \left(\frac{\beta}{k_0}\right)^2 = \frac{\varepsilon(\omega)}{1+\varepsilon(\omega)}\frac{\mu(\omega)-\varepsilon(\omega)}{1-\varepsilon(\omega)} = |\varepsilon(\omega)|\,\frac{|\varepsilon(\omega)|+\mu(\omega)}{\varepsilon^2(\omega)-1}} \tag{3.89}$$

3.4 Superficial Modes

Since the **cutoff** of the superficial modes is always verified when $\overline{n} = 1$, the dispersion diagram must always have values $\overline{n} \geq 1$. If we consider $F = 0.56$ and

$$X = \frac{1+\sqrt{1-4\,a\,F}}{2a} = \frac{2-F}{2\,a} = 2 \tag{3.90}$$

Then,

$$\begin{cases} \varepsilon(X) = -1 \\ \\ \mu(X) = -1 \end{cases} \tag{3.91}$$

$$\boxed{\varepsilon(X)\mu(X) = 1} \tag{3.92}$$

Leading us to

$$X = \frac{2 - F}{2\,a} = 2 \tag{3.93}$$

$$\begin{cases} \overline{n}^2 = -\frac{1}{2} \quad \text{TE Modes} \\ \\ \overline{n}^2 = -\frac{1}{2} \quad \text{TM Modes} \end{cases} \tag{3.94}$$

With this result, we can easily conclude that we can't have $\overline{n} = \infty$. Therefore, this value of X cannot allow propagation both of the TE and the TM modes. It's important to underline that, for the chosen values ($a = 0.36$ and $F = 0.56$), we get

$$2 - F = 1 + \sqrt{1 - 4\,a\,F} \tag{3.95}$$

And for

$$a\,X = 1 - 2\,a \rightarrow X = \frac{1 - \sqrt{1 - 4\,a\,F}}{2\,a} = \frac{F}{2\,a} = \frac{1}{a} = 0.7778 \tag{3.96}$$

$$\boxed{\varepsilon(X) = \mu(X) = 1 - X = 1 - \frac{F}{2\,a} = 3 - \frac{1}{a} = 0.2222} \tag{3.97}$$

Leading to

$$X = \frac{1 - \sqrt{1 - 4\,a\,F}}{2\,a} = \frac{1}{a} - 2 \tag{3.98}$$

$$\begin{cases} \overline{n} = 0 & \text{TE Modes} \\ \\ \overline{n} = 0 & \text{TM Modes} \end{cases} \tag{3.99}$$

That, once again, does not correspond to any propagation.

In fact, as seen before, the **TE** propagation is only possible when $\mu(X) < 0$ and $\overline{n} > 1$. While for $a = 0.36$ the TE modes are impossible, for other values of a, there is TE propagation.

From (3.85) and (3.64),

$$\overline{n}^2 = \frac{1 - \frac{F}{1-a\,X}}{1 + (1 - \frac{F}{1-a\,X})} \frac{(1 - X) - (1 - \frac{F}{1-a\,X})}{1 - (1 - \frac{F}{1-a\,X})} = \tag{3.100}$$

$$\overline{n}^2 = \frac{(a\,X + F - 1)(a\,X^2 - X + F)}{2\,F\,(a\,X + \frac{1}{2}(F - 2))} \tag{3.101}$$

Where $X = -(0.5/a)(F - 2)$ is the only resonance and, for our problem, $aX^2 + (F-1)\,X - F$ has the only valid root in $X = ((1-F) + \sqrt{(F-1)^2 + 4\,a\,F})/(2\,a)$. These results lead us to,

$0 < a < 0.36$		$\frac{(1-F)+\sqrt{(F-1)^2+4\,a\,F}}{2\,a}$; $-\frac{1}{2}\frac{F-2}{a}$	
$a = 0.36$	The TE modes are impossible for this value of a		
$a > 0.36$		$-\frac{1}{2}\frac{F-2}{a}$; $\frac{(1-F)+\sqrt{(F-1)^2+4\,a\,F}}{2\,a}$	

Table 3.8: Existence of TE modes for various values of a

And, these same results can be seen in the following figures after simulation

for some important values of a,

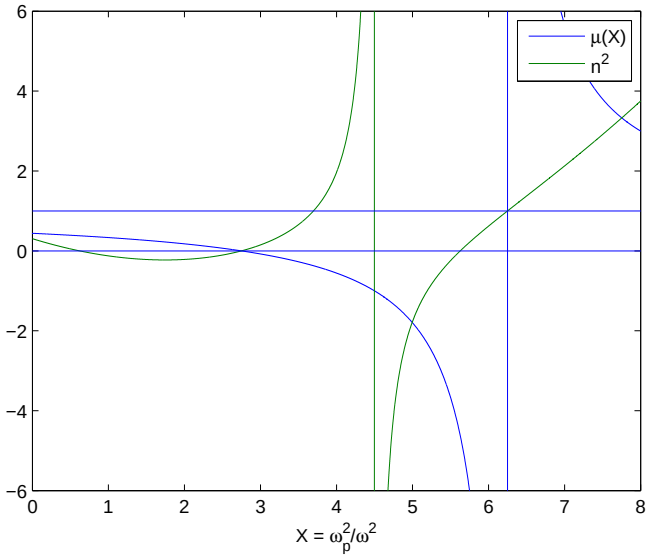

Figure 3.26: TE modes possibility for $a = 0.16$

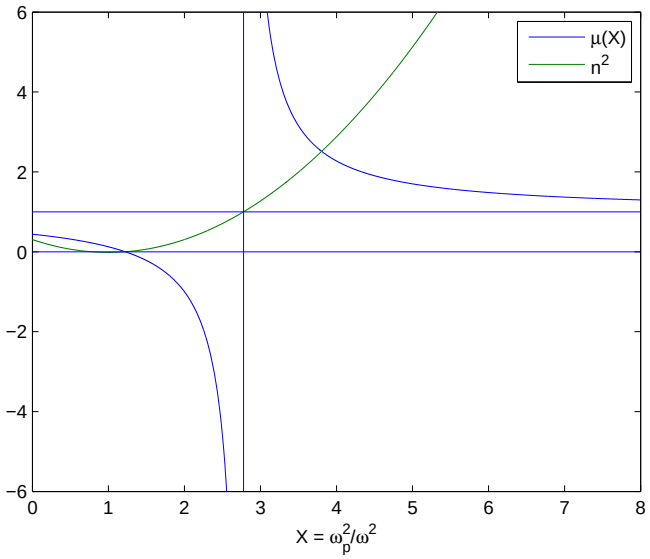

Figure 3.27: TE modes are impossible to propagate for $a = 0.36$

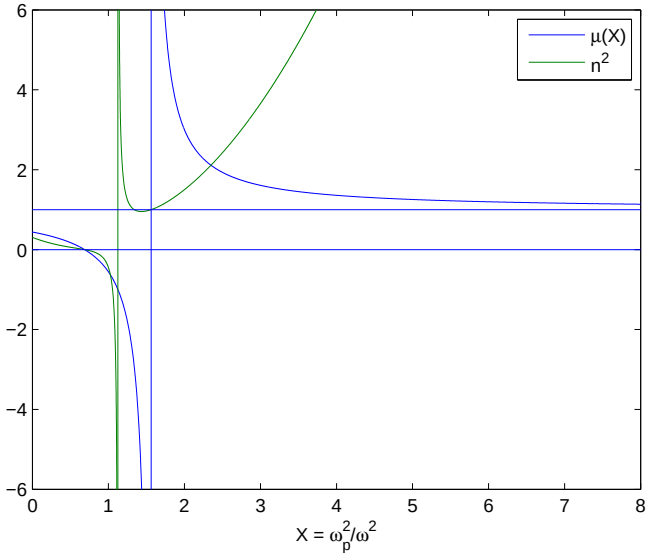

Figure 3.28: TE modes possibility for $a = 0.64$

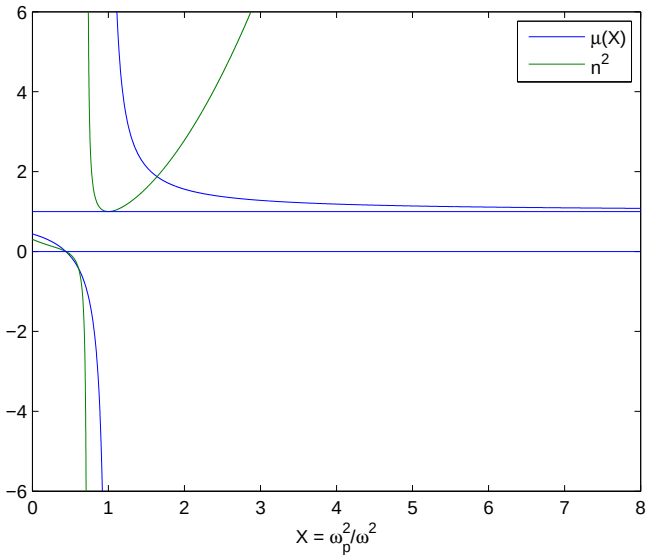

Figure 3.29: TE modes possibility for $a = 1.0$

If, instead of having a fixed value of F we consider $a = 0.36$, we have,

$0 < F < 0.56$		$\frac{-(F-1)+\sqrt{(F-1)^2+4\,a\,F}}{2\,a}$; $-\frac{1}{2}\frac{F-2}{a}$	
$F = 0.56$	The TE modes are impossible for this value of F		
$0.56 < F < 1$		$-\frac{1}{2}\frac{F-2}{a}$; $\frac{-(F-1)+\sqrt{(F-1)^2+4\,a\,F}}{2\,a}$	

Table 3.9: Existence of TE modes for various values of F

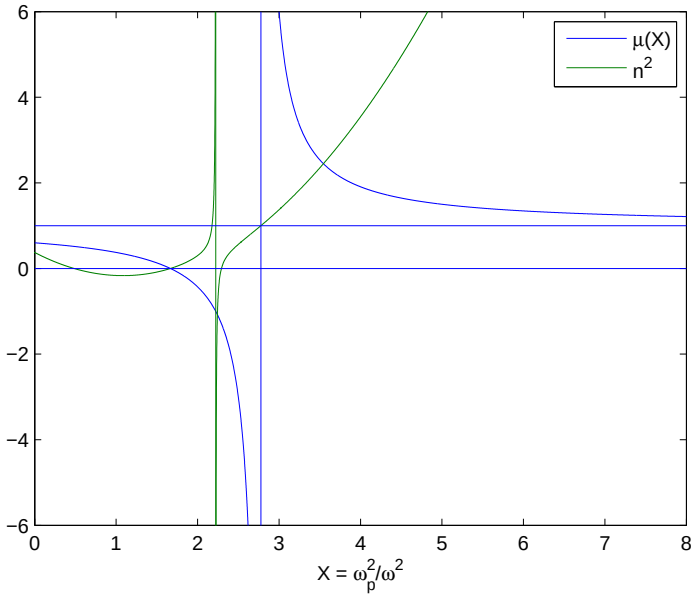

Figure 3.30: TE modes possibility for $F = 0.40$

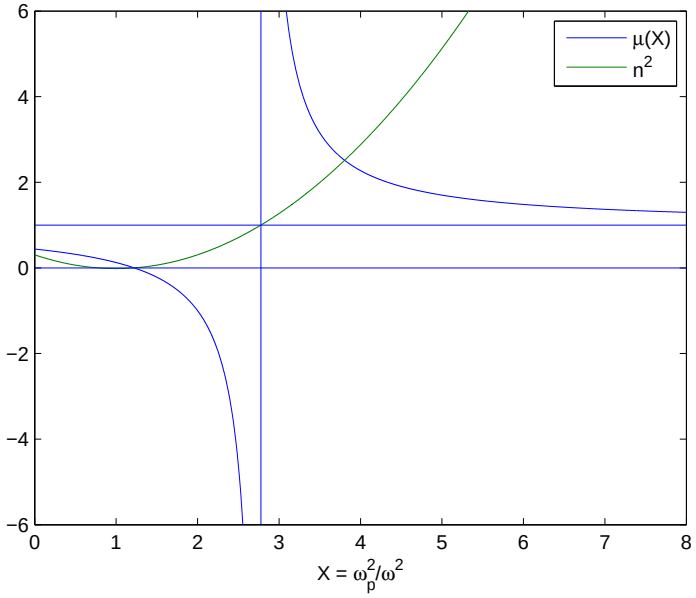

Figure 3.31: TE modes possibility for $F = 0.56$

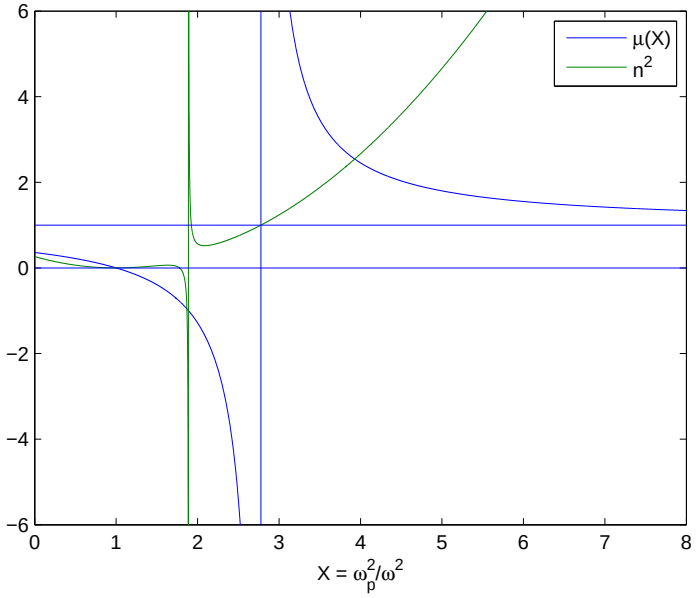

Figure 3.32: TE modes possibility for $F = 0.64$

From Table 3.8, Table 3.9 and the above simulations, we can conclude that there is always one TE mode propagating except when $a = 0.36$ and $F = 0.56$, where there aren't any TE modes propagating. This is a forward TE mode since it propagates in the DPS region.

The same analysis will be done for the **TM modes**, where propagation is only possible when $\varepsilon(X) < 0$ and $\overline{n} > 1$. From (3.89) and (3.64) we have

$$\overline{n}^2 = \left(\frac{1-X}{1+(1-X)}\right)\left(\frac{1-F\frac{1}{1-aX}-(1-X)}{1-(1-X)}\right) \tag{3.102}$$

$$\overline{n}^2 = \frac{(X-1)\left(a\,X^2 - X + F\right)}{X\,(X-2)\,(a\,X-1)} \tag{3.103}$$

There are three resonances in (3.103), $X = 0$, $X = 2$ and $X = 1/a$, but only the last two are valid to our problem since we don't consider a null frequency. The positive root is given by $X = ((1-F) + \sqrt{(F-1)^2 + 4\,a\,F})/(2\,a)$

For $F = 0.56$, we only have **TM modes** for:

$0 < a < 0.36$	$\left]\, 2\,;\, \frac{(1-F)+\sqrt{(F-1)^2+4\,a\,F}}{2\,a}\right[$ and $\left]\, \frac{1}{a}\,;+\infty\right[$
$a = 0.36$	$\left]\, \frac{1}{a}\,;+\infty\right[$
$0.36 < a < 1$	$\left]\, \frac{(1-F)+\sqrt{(F-1)^2+4\,a\,F}}{2\,a}\,;\, \frac{1}{a}\right[$ and $\left]\, 2\,;+\infty\right[$
$a \geq 1$	$\left]\, 2\,;+\infty\right[$

Table 3.10: Existence of TM modes for various values of a

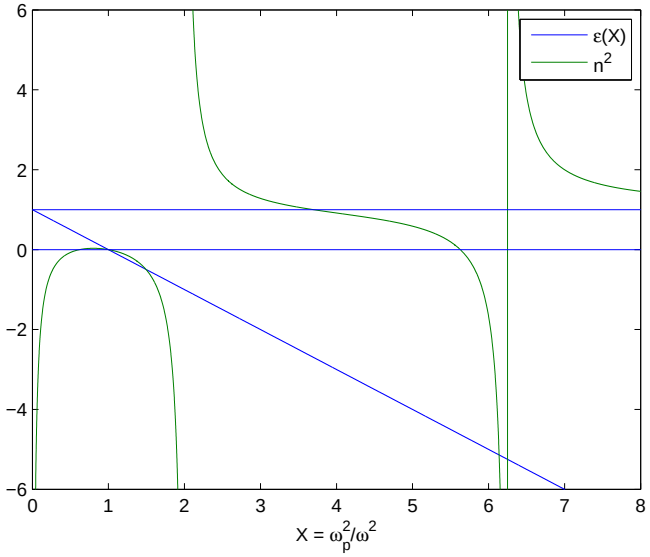

Figure 3.33: TM modes possibility for $a = 0.16$

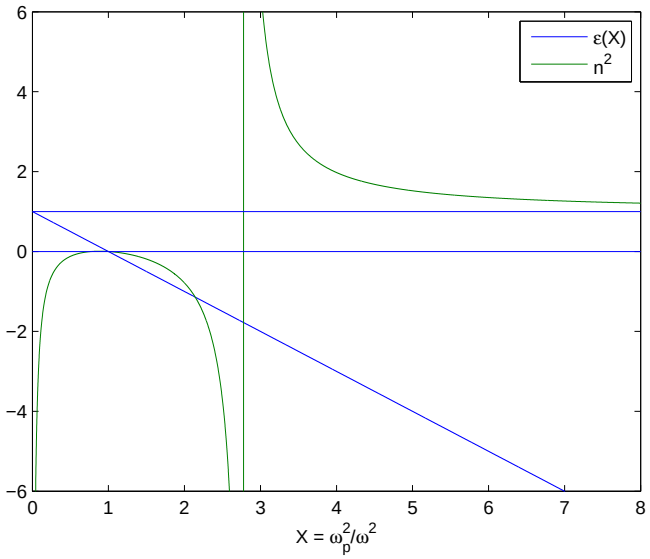

Figure 3.34: TM modes are impossible to propagate for $a = 0.36$

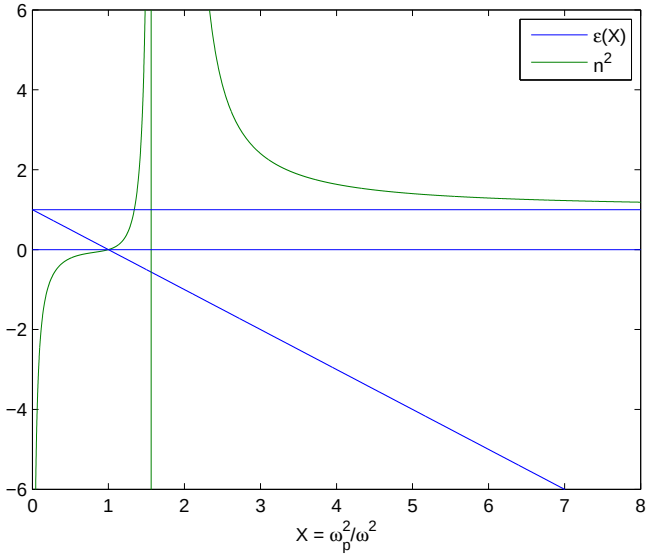

Figure 3.35: TM modes possibility for $a = 0.64$

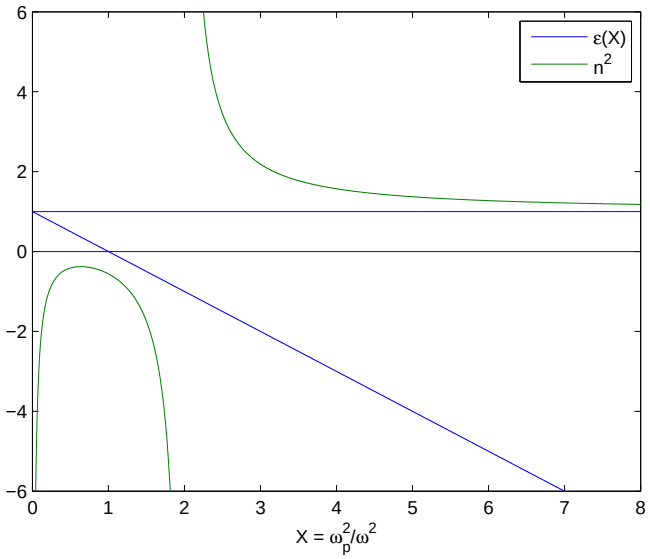

Figure 3.36: TM modes possibility for $a = 1.0$

From Table 3.10 and the above simulations, we can conclude that there are

two TM modes propagating when, $0 < a < 0.36$ or $0.36 < a < 1$, both ranges with $F = 0.56$. For values of a equal to 0.36 or greater than 1, just one TM mode propagates.

If, instead of having a fixed value of F we consider $a = 0.36$, we have,

$0 < F < 0.56$	$\left]\, 2\,;\, \frac{(1-F)+\sqrt{F^2-2F+4aF+1}}{2\,a} \right[$	and $\left]\, \frac{1}{a}\,;+\infty \right[$
$F = 0.56$	$\left]\, \frac{1}{a}\,;+\infty \right[$	
$0.56 < F < 1$	$\left]\, \frac{(1-F)+\sqrt{F^2-2F+4aF+1}}{2\,a}\,;\, 2 \right[$	and $\left]\, \frac{1}{a}\,;+\infty \right[$

Table 3.11: Existence of TM modes for various values of F

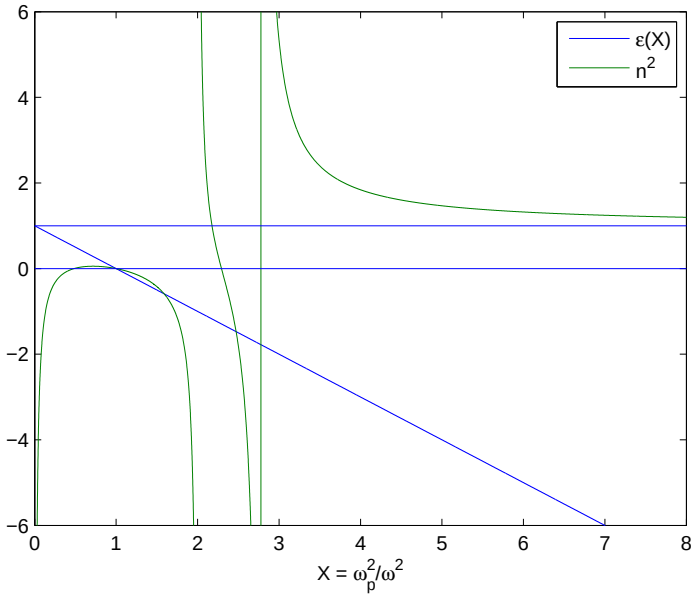

Figure 3.37: TM modes possibility for $F = 0.40$

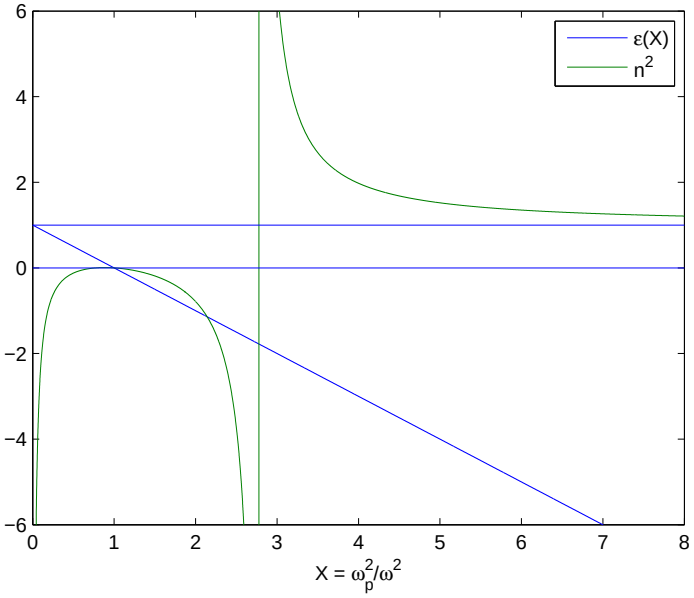

Figure 3.38: TM modes possibility for $F = 0.56$

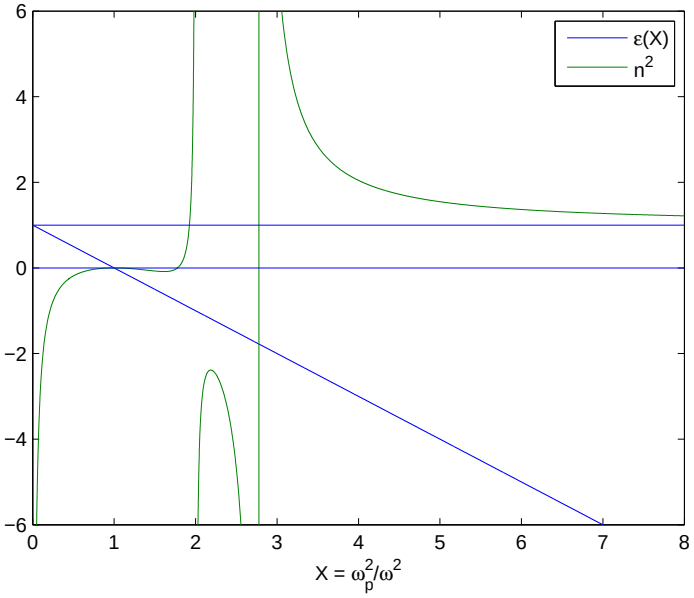

Figure 3.39: TM modes possibility for $F = 0.64$

Again, from Table 3.11 and the above simulations, we can conclude that there are two TM modes propagating when $F \neq 0.56$ and one TM mode propagating when $F = 0.56$. The forward TM mode appears in the DPS region and the backward TM mode propagates in the DNG region.

Chapter 4

Propagation on a DNG Slab

In this chapter we shall study the propagation of electromagnetic waves on a DNG slab waveguide. This structure is composed by a slab of DNG media, limited on the x axis, which is between two semi-infinite DPS media, like the following figure,

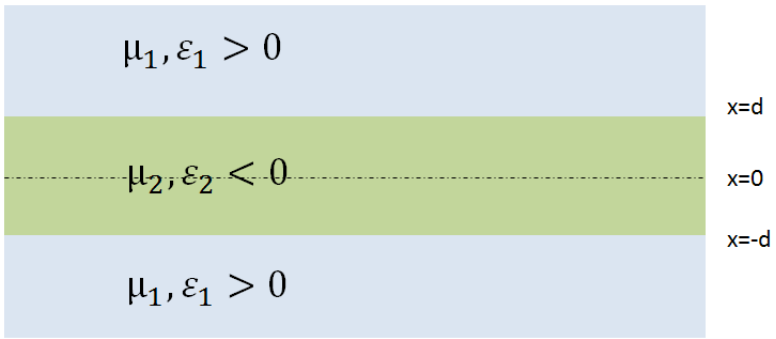

Figure 4.1: A DNG slab waveguide immersed on a DPS media

4.1 Modal Equations

As seen in the previous chapter, for the **TE modes**, the homogenous wave equation is given by,

$$\frac{\partial^2}{\partial x^2}\mathbf{E} + (k_0^2\, n_i^2 + \beta^2)\mathbf{E} = 0 \tag{4.1}$$

In the DNG medium, the solutions for this equation can take the following form,

$$\mathbf{E}_y(x) = E_{0e}\cos(h_2\, x) + E_{0o}\sin(h_2\, x) \tag{4.2}$$

With the transverse propagation constant h_2,

$$h_2 = \omega^2 \mu_2 \varepsilon_2 + \beta^2 \tag{4.3}$$

We can easily see that there are two kind of solutions in (4.2):

- An odd solution for $\sin(h_2\, x)$ term;
- An even solution for $\cos(h_2\, x)$ term.

Similarly to the previous chapter, we want the electric field decaying with the distance to x axis, so the evanescence of the electric field can be represented, in the DPS media, by,

$$\mathbf{E}_y(x) = \begin{cases} E_{01}\exp(i\, h_1\, x) & , x \geq d \\ \\ E_{02}\exp(-i\, h_1\, x) & , x \leq -d \end{cases} \tag{4.4}$$

With the transverse wave number given by,

$$h_i = i\,\alpha_i \tag{4.5}$$

And the attenuation constant, α_i, is defined by,

$$\alpha_i^2 = \beta^2 + k_0^2\, n_i^2 \tag{4.6}$$

Placing the attenuation constant in 4.4 we can establish for the evanescent fields the following expressions,

$$\mathbf{E}_y(x) = \begin{cases} E_{01}\exp(-\alpha_1\, x) & ,\, x \geq d \\ \\ E_{02}\exp(\alpha_1\, x) & ,\, x \leq -d \end{cases} \tag{4.7}$$

If we consider the beginning of the DPS medium as $|d|$ we can re-write (4.4) as

$$\mathbf{E}_y(x) = \begin{cases} E_{01}\exp[-\alpha_1\,(x-d)] & ,\, x \geq d \\ \\ E_{02}\exp[\alpha_1\,(x+d)] & ,\, x \leq -d \end{cases} \tag{4.8}$$

For the **odd mode** the electric fields has the relations,

$$E_y = \begin{cases} E_{01}\exp[-\alpha_1\,(x-d)] & ,\, x \geq d \\ \\ E_{0o}\sin(h_2\, x) & ,\, x \leq |d| \\ \\ E_{02}\exp[\alpha_1\,(x+d)] & ,\, x \leq -d \end{cases} \tag{4.9}$$

Since we chose the odd mode,

$$E_{0o} = -E_{01} \tag{4.10}$$

To obtain the expression for the magnetic field, we use the Maxwell–Faraday equation,

$$\nabla \times \mathbf{E} = i\omega\mu\mathbf{H} \tag{4.11}$$

With, as known,

$$\frac{\partial}{\partial z} \triangleq i\,\beta$$

We have,

$$\nabla \times \mathbf{E} = -\frac{i}{\omega\mu} \begin{vmatrix} \hat{x} & \hat{y} & \hat{z} \\ \frac{\partial}{\partial x} & 0 & i\,\beta \\ 0 & E_y & 0 \end{vmatrix} \tag{4.12}$$

And therefore

$$\mathbf{H} = -\frac{i}{\omega\mu}(-i\,\beta\,E_y\hat{x} + \frac{\partial E_y}{\partial x}\hat{z}) \tag{4.13}$$

Applying 4.13 in 4.9,

$$H_x = -\frac{\beta}{\omega\,\mu}\begin{cases} E_{01}\exp[-\alpha_1\,(x-d)] & ,\, x \geq d \\ E_{0o}\sin(h_2\,x) & ,\, x \leq |d| \\ E_{02}\exp[\alpha_1\,(x+d)] & ,\, x \leq -d \end{cases} \tag{4.14}$$

$$H_z = -\frac{i}{\omega\,\mu}\begin{cases} -E_{01}\alpha_1\exp[-\alpha_1\,(x-d)] & ,\, x \geq d \\ E_{0o}h_2\cos(h_2\,x) & ,\, x \leq |d| \\ E_{02}\alpha_1\exp[\alpha_1\,(x+d)] & ,\, x \leq -d \end{cases} \tag{4.15}$$

To assure the continuity of the fields, we apply the boundary conditions at the interface $x = d$, and obtain,

$$E_y(x = d^-) = E_y(x = d^+) \tag{4.16}$$

$$H_z(x = d^-) = H_z(x = d^+) \tag{4.17}$$

Leading to,

$$E_{0o}\sin(h_2 d) = E_{01} \tag{4.18}$$

$$\frac{1}{\mu_2}E_{0o}h_2\cos(h_2 d) = -\frac{E_{01}}{\mu_1}\alpha_1 \tag{4.19}$$

$$\begin{bmatrix} \sin(h_2 d) & -1 \\ \frac{h_2 \cos(h_2 d)}{\mu_2} & \frac{\alpha_1}{\mu_1} \end{bmatrix} \begin{bmatrix} E_{0o} \\ E_{01} \end{bmatrix} = 0 \tag{4.20}$$

$$\frac{\alpha_1}{\mu_1}\sin(h_2 d) + \frac{h_2}{\mu_2}\cos(h_2 d) = 0 \tag{4.21}$$

Giving us the asymmetric or **odd TE modal equation,**

$$\alpha_1 = -h_2 \frac{\mu_2}{\mu_1}\cot(h_2 d) \tag{4.22}$$

Similarly, to the even solution of the wave equation, we obtain the even or **symmetric TE modal equation,**

$$\alpha_1 = h_2 \frac{\mu_2}{\mu_1}\tan(h_2 d) \tag{4.23}$$

We obtain the modal equations for the slab for both **TE mode**s,

$$\begin{cases} \alpha_1 = -h_2 \frac{\mu_1}{\mu_2}\cot(h_2 d) & \text{(Odd Modes)} \\ \\ \alpha_1 = h_2 \frac{\mu_1}{\mu_2}\tan(h_2 d) & \text{(Even Modes)} \end{cases} \tag{4.24}$$

Repeating the same kind of procedure to the **TM mode**s,

$$\begin{cases} \alpha_1 = -h_2 \frac{\varepsilon_1}{\varepsilon_2}\cot(h_2 d) & \text{(Odd Modes)} \\ \\ \alpha_1 = h_2 \frac{\varepsilon_1}{\varepsilon_2}\tan(h_2 d) & \text{(Even Modes)} \end{cases} \tag{4.25}$$

Considering,

$$a = \alpha_1 d \tag{4.26}$$

$$b = h_2 d \tag{4.27}$$

We can simplify the modal equations. For the **TE mode,**

$$\begin{cases} a = -b\,\frac{\mu_1}{\mu_2}\cot(b) & \text{(assymetric mode)} \\ \\ a = b\,\frac{\mu_1}{\mu_2}\tan(b) & \text{(symmetric mode)} \end{cases} \tag{4.28}$$

And for the **TM mode**,

$$\begin{cases} a = -b\,\frac{\varepsilon_1}{\varepsilon_2}\cot(b) & \text{(assymetric mode)} \\ \\ a = b\,\frac{\varepsilon_1}{\varepsilon_2}\tan(b) & \text{(symmetric mode)} \end{cases} \tag{4.29}$$

The relation between the normalized propagation's constants is given by:

$$a^2 + b^2 = V^2 \tag{4.30}$$

Where V, the normalized frequency, is given by,

$$V = k_0 d\sqrt{\varepsilon_2\mu_2 - \varepsilon_1\mu_1} \tag{4.31}$$

The intersection of the curve (4.30) with the modal equations will represent the modal solutions for these modes in the slab.

4.2 Surface Mode Propagation

In this section we shall analyze the surface modes on the DNG slab. From (4.3), h_2 is real when,

$$\beta < \omega \sqrt{\varepsilon_2 \mu_2} \tag{4.32}$$

And has imaginary values when,

$$\beta > \omega \sqrt{\varepsilon_2 \mu_2} \tag{4.33}$$

If we assume either imaginary or real values of h_2, in the analysis of the DNG slab, we still maintain the surface mode conditions where the wave diminishes with the distance away from the slab. If we consider the following relations,

$$\tan(i\,x) = i\tanh(x) \tag{4.34}$$

$$\cot(i\,x) = -i\coth(x) \tag{4.35}$$

And assuming that

$$B = -i\,b \tag{4.36}$$

We are able to rewrite equations (4.28) and (4.30) to,

$$\begin{cases} a = -B\,\frac{\mu_1}{\mu_2}\coth(B) & \text{(Assymetric mode)} \\ \\ a = -B\,\frac{\mu_1}{\mu_2}\tanh(B) & \text{(Symmetric mode)} \end{cases} \tag{4.37}$$

And

$$a^2 = B^2 + V^2 \tag{4.38}$$

The numerical solutions of the equations can be found, both in plane (b, a) or (B, a), through the intersection of the corresponding modal curves and the

ones representing equations (4.30) and (4.38).

First we will study the DPS situation with $\varepsilon_1 = 1$, $\mu_1 = 1$, $\varepsilon_2 = 2$ and $\mu_2 = 2$.

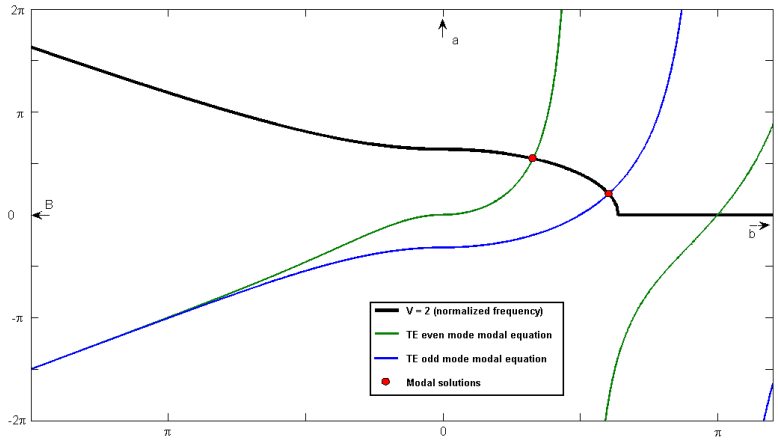

Figure 4.2: The modal solutions (red dots) for a conventional DPS dielectric slab with $\varepsilon_1 = 1$, $\mu_1 = 1$, $\varepsilon_2 = 2$ and $\mu_2 = 2$.

The horizontal positive semi-axis represents the transverse wave number, b, while the negative semi-axis represents the imaginary part, previously called B. As expected, in a DPS slab, there are only modal solutions with real b.

However, if we consider a DNG slab, there are solutions with imaginary b. This result can be seen in Figure 4.3.

These modes are called **super-slow modes** since the phase velocity, given by $v_p = \omega/\beta$, is lower than the speed of light in the outer medium,

$$v_p < \frac{c}{\sqrt{\varepsilon_1 \mu_1}} \tag{4.39}$$

Then again, with a real value of b, the superficial modes are called **slow**

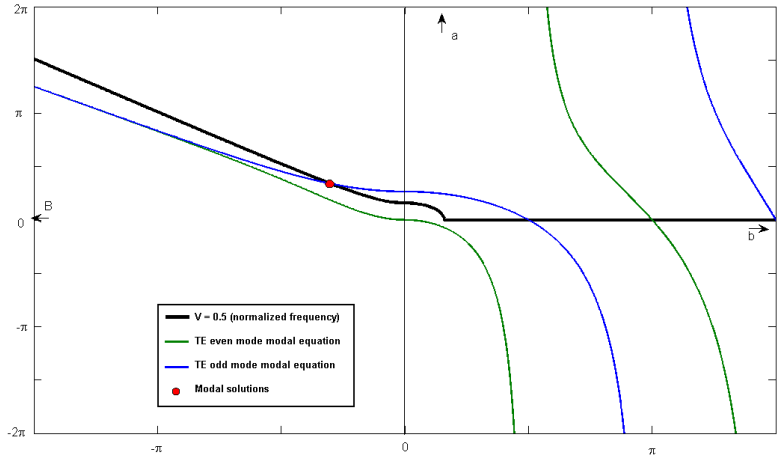

Figure 4.3: The modal solutions (red dots) for a DNG slab with $\varepsilon_1 = 1$, $\mu_1 = 1$, $\varepsilon_2 = -1.5$, $\mu_2 = -1.5$ and $V = 0.5$.

modes, and one easily verify that the phase velocity assumes a value within

$$\frac{c}{\sqrt{\varepsilon_2 \mu_2}} < v_p < \frac{c}{\sqrt{\varepsilon_1 \mu_1}} \tag{4.40}$$

Since we have a DNG medium in the slab, the sign of the right hand side of the TE modal equations changes due to $\mu_2 < 0$. This inversion in the signal of the modal equations causes a change in the slope of the branches of tangent and cotangent function and, for a given range of frequencies, we also have some slow-modes that can have more than one solution for the same $h_2 d$, as we can see on Figure 4.4. Has seen before, the electric field E_y of the even slow modes varies with a cosine function. On the other hand, the electric field E_y of the odd slow modes varies with the a sine function. But, if we have an imaginary wave number, both trigonometric functions become hyperbolic functions. When the inner medium is more dense than the outer medium, there are slow modes and,

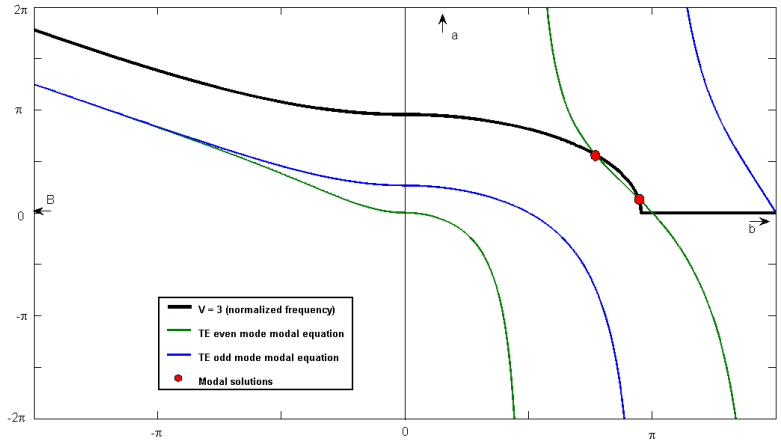

Figure 4.4: The modal solutions (red dots) for a DNG slab with $\varepsilon_1 = 1$, $\mu_1 = 1$, $\varepsilon_2 = -1.5$, $\mu_2 = -1.5$ and $V = 3$

given a DNG metamaterial inner medium, also originates super slow modes.

To describe the transitions between the slow modes and the the super slow modes, we have the following relations. For the even modes,

$$\cos^2(b) + \left(\frac{\mu_1}{|\mu_2|}\right)^2 \left[\sin^2(b) + b\tan(b)\right] = 0 \tag{4.41}$$

And, for odd modes, we have,

$$\sin^2(b) + \left(\frac{\mu_1}{|\mu_2|}\right)^2 \left[\cos^2(b) + b\cot(b)\right] = 0 \tag{4.42}$$

The representation of the dispersion diagram for the TE modes of the DNG dielectric slab, with $\varepsilon_1 = 1$, $\mu_1 = 1$, $\varepsilon_2 = -1.5$, $\mu_2 = -1.5$, is shown in Figure 4.5. The dashed lines, defined by k_0 as a function of βd, represent the transition limits. The first one, with a higher slope, defined by

$$k_0 d = \frac{\beta d}{\sqrt{\varepsilon_1 \mu_1}} \tag{4.43}$$

represents the cutoff condition of the surface modes on the slab, where $h_1 d =$

0. The second dashed line, whith lower slope, given by

$$k_0 d = \frac{\beta d}{\sqrt{\varepsilon_2 \mu_2}} \tag{4.44}$$

expresses the transition between the super slow modes and the slow modes.

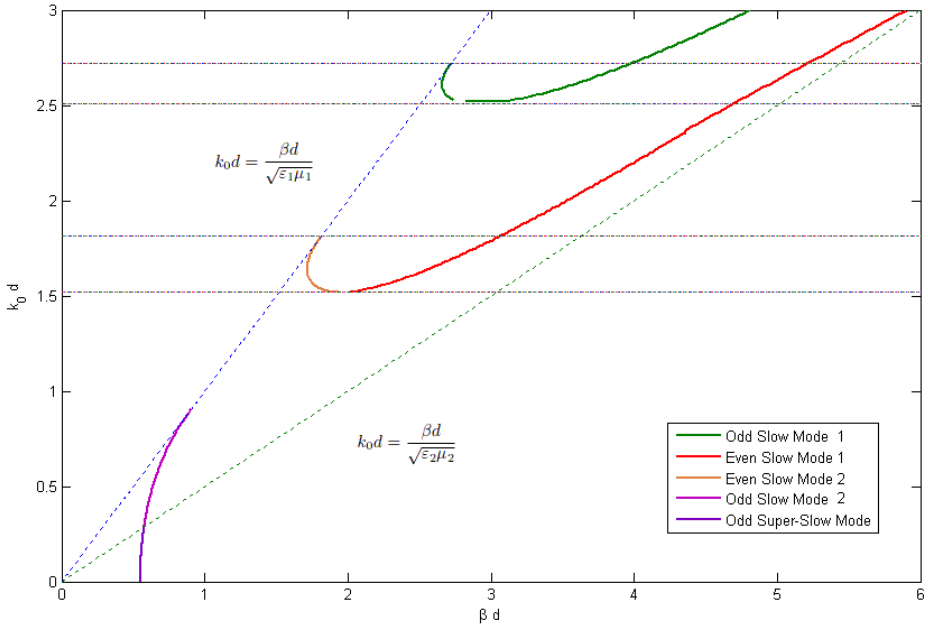

Figure 4.5: Dispersion diagram for the TE modes of the DNG slab with $\varepsilon_1 = 1$, $\mu_1 = 1$, $\varepsilon_2 = -2$ and $\mu_2 = -2$

Two degenerated modes are excited in the dielectric slab, a conventional mode and a limited conventional mode has we can verify in Figure 4.5.

The odd super-slow mode is the fundamental mode, which is the first one since because it's excited from null frequency, and becomes a slow mode when $V = \mu_1 / |\mu_2|$ and propagates until $V = \pi/2$.

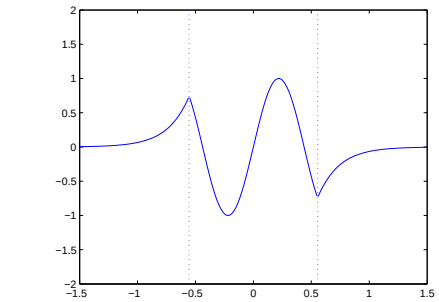

i)

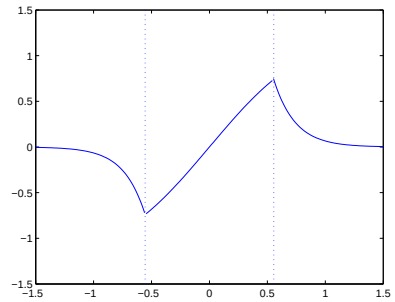

ii)

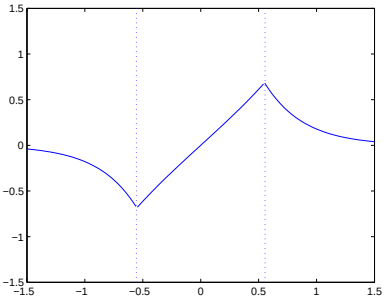

iii)

Figure 4.6: Electric Field for odd TE modes with $\varepsilon_1 = 1$, $\mu_1 = 1$, $\varepsilon_2 = -2$ and $\mu_2 = -2$ for **(i)** Odd slow mode 1 **(ii)** Odd slow mode 2 **(iii)** Odd super-slow mode

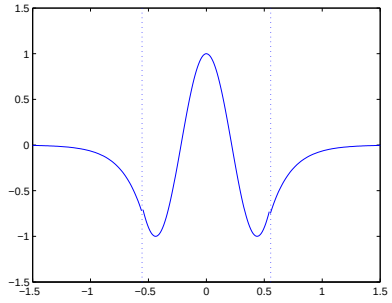

i)

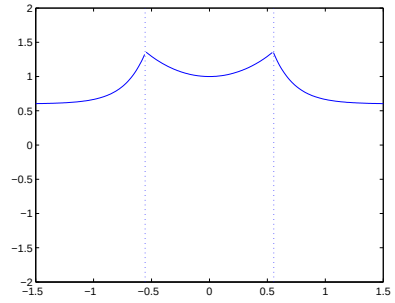

ii)

Figure 4.7: Electric Field for even TE modes with $\varepsilon_1 = 1$, $\mu_1 = 1$, $\varepsilon_2 = -2$ and $\mu_2 = -2$ for **(i)** Even slow mode 1 **(ii)** Even slow mode 2

With this DNG slab structure, where we assumed $\mu_1\varepsilon_1 < \mu_2\varepsilon_2$, we can conclude that there is a direct relation between the constitutive parameters and

the resultant dispersive diagram, as the point from which the fundamental mode transitions from a super-slow mode to a slow-mode depends on the value of both μ_1 and μ_2. But if we consider the case $\mu_1\varepsilon_1 < \mu_2\varepsilon_2$, when slab's inner medium is less dense than the outer medium, there are several important results.

Using the expression of the relation for the outer medium,

$$\alpha_1^2 = \beta^2 - \omega^2\varepsilon_1\mu_1$$

and ensuring $a \geq 0$ for the electric slab, we get the following inequality,

$$B^2 + V^2 \geq 0 \tag{4.45}$$

Where, from expression (4.31), we obtain

$$V^2 < 0 \tag{4.46}$$

Although the expression (4.45) is only verified when we have a super-slow mode, otherwise we would get $-b^2 + \left|v^2\right| \geq 0$, which is always untrue. With this result, while still considering the situation where the outer medium is more dense than the slab's inner medium, we have from (4.30),

$$a^2 + b^2 < 0 \tag{4.47}$$

We can conclude, from equations (4.46) and (4.47), that the following relation must be verified in order to have propagation in the slab,

$$b^2 < 0 \tag{4.48}$$

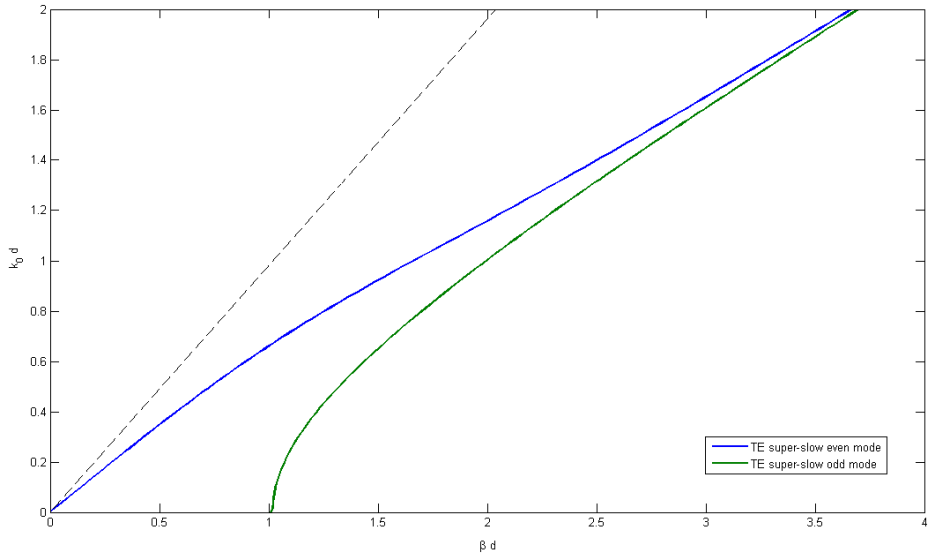

Figure 4.8: DNG dielectric slab dispersion diagram with $\varepsilon_1 = 2$, $\mu_1 = 1$, $\varepsilon_2 = -1$ and $\mu_2 = -1.5$

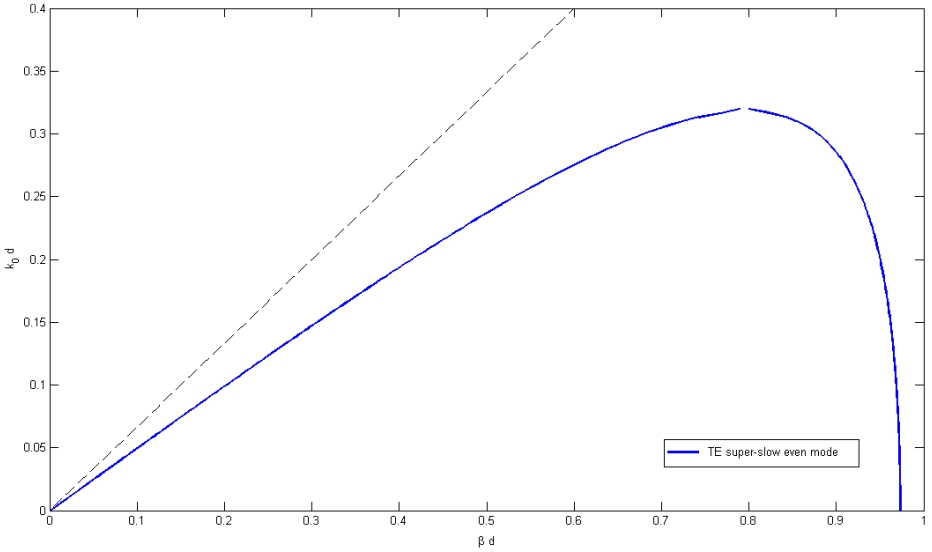

Figure 4.9: DNG dielectric slab dispersion diagram with $\varepsilon_1 = 2$, $\mu_1 = 2$, $\varepsilon_2 = -1$ and $\mu_2 = -1.5$

Only in the presence of super-slow modes, these conditions are valid. This

result can be verified on Figure 4.8, where we verify (4.45), (4.47) and (4.48). As expressed in (4.46), the propagation in a less dense medium is only possible if we are in the presence of super-slow modes. This is only satisfied using a DNG dielectric slab.

In the case of a less dense inner medium, we can have two different dispersion diagram cases:

- One where $|\mu_2| > \mu_1$, shown in Figure 4.8;
- One where $|\mu_2| < \mu_1$, shown in Figure 4.9.

In the first case, 4.8, there is propagation of an even and an odd super-slow mode. Both this modes have a null cutoff frequency and a longitudinal wave number, β, that tends to the same value while increasing the frequency.

In the second case, Figure 4.9, only the even super slow mode propagates and it's limited by frequency. While on this frequency band, there are always two solutions that tend to the same value. The point where the double-solutions intersect represents the limit from which there is no surface mode propagation on the DNG slab. We can also conclude that there are propagation conditions for super slow modes, for all values of k_0.

Chapter 5

Conclusions

Being this the final chapter, we shall gather the main conclusions of the present work. Some suggestions for future work is presented and potential applications as well.

5.1 Summary

In the first chapter, a brief historical background and framework about DNG metamaterials is introduced and the first experimental demonstrations of the electromagnetic properties of DNG metamaterials is presented as well. The state of the art follows describing some present works and current investigation. The motivation to this work and objectives of this dissertation are revealed, where the interest for this subject is explained. Finally, the original contributions of the present dissertation to the subject are described.

In the second chapter we made a media classification, based on the permeability and permittivity, and studied electromagnetic proprieties of a DNG metamaterial. A DNG medium presents negative permeability and negative permittivity. These leads to negative refraction index and to existence of waves

that have wave vector and energy flow propagating in an antiparallel direction, these waves are known has Backward Waves. If both the permeability and the permittivity are negative, we have fundamental problems since we can't have negative energy density, this proves that a DNG medium is necessarily dispersive due to the definition of electromagnetic energy. Therefore a study to the dispersion and to the Lorentz Dispersive Model is done. Since the dispersion is intrinsically connected to loses, we also concluded that, not only the group velocity has different value of the phase velocity, but also has opposite direction in a DNG media.

In the third chapter we studied and analyzed and unbounded interface between a DNG medium and a DPS medium. The Maxwell's equations are applied to the plane waves propagating in the isotropic and unbounded DNG medium and some results, like the homogeneous wave equations, are shown. The constitutive relations for this medium were calculated and then a modal analysis is done, revealing that this interface allows both TE and TM surface modes wave propagation. These propagation modes are not possible in an ordinary DPS wave guiding structure. The dispersion in the DNG metamaterial is included recurring to the Lorentz Dispersive Model. In the lossless case, when $\mu_2/\mu_1 = -1$ and $\varepsilon_2/\varepsilon_1 = -1$, for TE mode and TM mode, respectively, there is no physical solution since the dispersion relation tends to infinitive. However, when considering a dispersive lossy model, physical solutions arise. The electric field, as function of frequency and distance, for TE modes, is shown, revealing that the electric field in the DNG medium is greatly affected by the variation of frequency. In both cases, the DNG and the DPS, the electric fields decays with considerable attenuation with the distance.

For a more practical view of the DNG-DPS interface, a less theoretical problem is studied. The problem is formulated assuring that resonances of both the

permeability and permittivity are close enough, which is one of the main problems when creating these new materials. Some simulations are obtained for various values of filling factor, leading, in specific cases, to two TM modes, one forward in the DPS zone and one backward in the DNG zone.

In the fourth chapter an analysis to the guided propagation on a DNG slab is done. This chapter has special interest since the construction of guided waveguides may be one of the greatest applications to DNG metamaterials. Like in the previous chapter, this structure also reveled the possibility of having surface wave mode propagation. However, the most important result is the propagation of super-slow modes, a consequence of the phase velocity in the inner medium (DNG medium) being smaller than in the outer medium (DPS medium). The surface slow modes reveal a double solution for a restricted frequency domain. The existence of these super-slow modes allows the propagation on the DNG slab even when a less dense medium for the slab is used, compared to the outer medium, $\mu_1\varepsilon_1 > \mu_2\varepsilon_2$. This phenomenon can only be verified on double negative materials. Analyzing the dispersion relation diagrams when the slab medium is less dense than the outer medium, we could see that, for a medium with $|\mu_2| < \mu_1$, there are two super-slow modes. For a medium with $|\mu_2| > \mu_1$, in a limited frequency band, only one super-slow mode propagates, however, in this band, there are always two possible modal solutions.

5.2 Future Work

The introduction of metamaterials in the electromagnetic panorama, brought new problems never before deemed possible.

Studying indefinite media, also considered metamaterials, should be considered since they are more general than DNG metamaterials, which are isotropic media. This would allow to study anisotropic metamaterials.

The present work analyzed two simple waveguiding structures with DNG media but there is a set of other structures with DNG, a set at least as large as the number of DPS structures. Their analysis should include the study of reflection and transmission factors.

One of the main applications DNG metamaterais are the lenses, from flat lens to superlenses, which can have a spatial resolution below that of the wavelength. Lenses with DNG media are very useful for high-gain antennas.

Bibliography

[1] P. Moller, B. Kramer, "Review: Electric fish", *BioScience* (American Institute of Biological Sciences) 41 (11), pp. 794–796, 1991.

[2] T. H. Bullock, *Electroreception*, Springer, pp. 5–7, 2005.

[3] *The Encyclopedia Americana; A Library Of Universal Knowledge*, New York: Encyclopedia Americana Corp, 1918.

[4] J. Stewart, *Intermediate Electromagnetic Theory*, World Scientific, pp. 50, 2001.

[5] A, Frood, *Riddle of 'Baghdad's batteries'*, BBC, 2003.

[6] B. Baigrie, *Electricity and Magnetism: A Historical Perspective*, Greenwood Press, pp. 7–8, 2006.

[7] G. Chalmers, "The lodestone and the understanding of matter in seventeenth century England", *Philosophy of Science 4* (1), pp. 75–95, 1937.

[8] J. Srodes, *Franklin: The Essential Founding Father*, Regnery Publishing, 2002.

[9] M. Uman , *All About Lightning*, Dover Publications, 1987.

[10] R. S. Kirby, *Engineering in History*, Courier Dover Publications, 1990.

[11] W. Berkson, *Fields Of Force: The Development Of A World View From Faraday To Einstein*, Routledge, pp.148, 1974.

[12] J. C. Maxwell, *A Treatise On Electricity And Magnetism*, Oxford Clarendon Press, Volume 1, 1873.

[13] H. A. Lorentz, A. Einstein, H. Minkowski, H. Weyl, *The Principle of Relativity*, Dover Publications, New York, 1952.

[14] *Electromagnetism, Maxwell's Equations, and Microwaves*, IEEE Virtual Museum, 2011.

[15] A. Sihvola, "Metamaterials in electromagnetics", *Metamaterials*, vol. 1, pp. 2-11, 2007.

[16] S. Zouhdi, A. Sihvola, M. Arsalane (Eds.), Advances in electromagnetics of complex media and metamaterials, *Kluwer Academic Publishers*, Dordrecht, vol. 89, pp. 1–17, 2003.

[17] J. C. Bose, "On the rotation of plane of polarisation of electric waves by a twisted structure", *Proc. Roy. Soc.*, vol. 63, pp. 146-152, 1898.

[18] D. T. Emerson, "The work of Jagadis Chandra Bose: 100 years of millimeter-wave research", *IEEE Trans. Microwave Theory and Techniques*, vol. 45, no. 12, pp. 2267-2273, 1997.

[19] I. V. Lindell, A. H. Sihvola, J. Kurkijirvi, Karl F. Lindman, "The last Hertzian and a harbinger of electromagnetic chirality", *The Radioscientist*, vol. 3, o. 2, pp. 38, 44-48, 52-53, June 1992.

[20] W.E. Kock, "Metallic Delay Lenses", *Bell. Sys. Tech. Jour. 27*, pp. 58–82, 1948.

[21] V. G. Veselago, "The electrodynamics of substances with simultaneously negative values of ε and μ", *Sov. Phys. Uspekhi*, vol. 10, no. 4, pp. 509-514, 1968. [Usp. Fiz. Nauk, vol. 92, pp. 517-526, 1967.]

[22] J. B. Pendry, A. J. Holden, D. J. Robbins, W J. Stewart, "Magnetism from conductors and enhanced non-linear phenomena", *IEEE Trans. Microwave Theory Tech.*, MTT-47, pp. 195, 1999.

[23] Smith, D.R., et al., "Composite medium with simultaneously negative permeability and permittivity", *Phys. Rev. Lett.*, vol. 84, no. 18, pp. 4184-4187, 2000.

[24] Shelby, R.A., et al., "Microwave transmission through a two-dimensional, isotropic, left-handed metamaterial", *Appl. Phys. Lett.*, vol. 78, no. 4, 2001, pp. 489-491.

[25] C. Caloz, C. C. Chang, T. Itoh, "Full-wave verification of the fundamental properties of left-handed materials in waveguide configurations", *J. Appl. Phys. 90*, 2001.

[26] G. V. Eleftheriades, A. K. Iyer, P. C. Kremer, "Planar negative refractive index media using periodically L-C loaded transmission lines", *IEEE Transactions on Microwave Theory and Techniques 50*, 2002.

[27] C. Caloz, T. Itoh, . *Application of the Transmission Line Theory of Left-handed (LH) Materials to the Realization of a Microstrip*

'LH line', IEEE Antennas and Propagation Society International Symposium 2, 2002.

[28] A. L. Topa, C. R. Paiva, and A. M. Barbosa, "Novel propagation features of double negative H-guides and H-guide couplers" - *Microwave And Optical Technology Letters,* Vol. 47, No. 2, pp. 185 - 190, October 20 2005.

[29] J. R. Canto, S. A. Matos, A. L. Topa, and C. R. Paiva, "Comportamento dispersivo de modos leaky em guias metamateriais DNG", *Proc Encuentro Ibérico de Electromagnetismo Computacional - EIEC* , Seia, Portugal, vol. 1, pp. 29 - 32, Sep. 2005.

[30] J. R. Canto, S. A. Matos, C. R. Paiva, and A. M. Barbosa, "Effect of losses in a layered structure containing DPS and DNG media", *Piers Online*, Vol. 4, No. 5, pp. 546 - 550, 2008.

[31] S. A. Matos, J. R. Canto, C. R. Paiva, and A. M. Barbosa, "Complex aberration effect in moving dispersive DNG media: A spacetime algebra approach", *Piers Online*, Vol. 4, No. 6, pp. 611 - 614, 2008.

[32] A. L. Topa, C. R. Paiva, and A. M. Barbosa, "Dispersion and losses in metamaterial DNG", *S. Zouhdi et al. (eds.), Metamaterials and Plasmonics: Fundamentals Modelling*, Applications, Springer Science + Business Media B.V, pp. 289 - 298, 2009.

[33] C. Soukoulis, *Metamaterials Found To Work For Visible Light*, DOE / Ames Laboratory, 2007.

[34] K. Bourzac, "A practical way to make invisibility cloaks", *Technology Review - MIT*,

http://www.technologyreview.com/computing/37720/page1/ , 2011.

[35] D. K. Cheng, *Field and Wave Electromagnetics*, Addison-Wesley, 1989.

[36] C. R. Paiva, *Meios Duplamente Negativos (DNG),* DEEC-IST, 2008.

[37] D. R. Smith and N. Kroll, "Negative refractive index in left-handed materials", *Phys. Rev. Lett.*, vol. 85, pp. 2933-2936, October 2000.

[38] Jin Au Kong, *Electromagnetic Wave Theory*, EMW publishing, Cambridge, Massachusetts, USA, 2008.

[39] L. Solymar, E. Shamonina, *Waves in Metamaterials*, Oxford University Press, 2009.